Final report

Using microwave to detect foreign objects in meat

Project code: V.TEC.1710

Prepared by: J. Marimuthu, V. Pamarla, R. Karayakallile Abraham
Murdoch University

Date published: 30 June 2021

PUBLISHED BY
Meat & Livestock Australia Limited
PO Box 1961
NORTH SYDNEY NSW 2059

Meat & Livestock Australia acknowledges the matching funds provided by the Australian Government to support the research and development detailed in this publication.

Abstract

The ability of a two-dimensional microwave imaging system to detect plastic physical foreign object contaminants within beef on an industrial based conveyor system was assessed. An automated planar ultra-wideband microwave scanning system with industrial food grade conveyor was designed and fabricated at Murdoch University. The system has ability to adopt various numbers of antennas (4 to 32) and different type of the antennas (Vivaldi Patch, Horn). Eight Vivaldi Patch Antennas or Horn antennas were connected to two Keysight Vector Network Analysers to generate the ultra-wideband step-frequency microwave signals, operating within the 300kHz to 6.5GHz frequency range. The network analysers were connected to an OptiPlex 7070 computer system to allow synchronisation, data acquisition and image formation.

Two experiments were performed. Experiment 1 assessed microwave detection of plastic within boxed meat. Three different phantoms of varying lean meat to fat ratios were constructed, 100% lean, 80% lean + 20% fat, and 60% lean + 40% fat. Within these phantoms three different configurations of embedding plastic were tested to assess different plastic sizes and locations within the boxed meat. Microwave scanning on the boxed meat was performed using an array of 4 antennas.

Experiment 2 assessed microwave detection of plastic in unboxed meat on a food grade automated conveyor system. Within chunks of meat distributed along a conveyor belt, two configurations of plastic foreign bodies were assessed, visible or non-visible. The meat was scanned by an array of 8 antennas as it moved along a conveyor belt.

Two different algorithms for image analysis were developed, confocal imaging techniques and Truncated Singular Value Decomposition (TSVD). The algorithms were created based on the permittivity and conductivity of the penetrating microwave signal and reflected back from the phantom. The reflected microwave signals were detected and transformed into a colour image based on the different contrasts within the tested platform. The confocal imaging technique with optimisation-based propagation techniques and TSVD were successful at creating an image with high contrast between the plastic and the surrounding with meat samples. The only limitation to this image was the presence of some shadowing around the plastic, which we expect to resolve through altered antenna-array design and improved imaging analysis.

Executive summary

- Microwave array using a confocal imaging technique successfully detected plastic embedded within boxed meat trim containing between 60 – 95% chemical lean.
- Microwave array using a confocal imaging technique with optimisation-based propagation successfully detected non-visible plastic embedded within loose beef meat chunks on a conveyor belt running at commercial speeds.
- Microwave array using Truncated Singular Value Decomposition (TSVD) successfully detected visible plastic embedded within loose beef meat chunks on a conveyor belt running at commercial speeds.

Table of contents

1. Introduction

Meat contamination with physical contaminants/hazards (foreign bodies) is a major challenge to meat safety. Safety and traceability of meat is one of the most important issues for marketers to ensure consumer protection and avoid costly recalls and damage to brand reputation. A physical contaminant to meat is defined as 'additional matter or alien objects not normally existing in food that could cause injury, disease or psychological trauma' (Aladjadjiyan, 2006). The major physical contaminant hazards are bone, plastic, insects, metal, glass, wood, rubber, hair, paper and fabric (Aladjadjiyan, 2006; Cavalheiro, da Silva, Leite, da Silva Felix, Herrero, & Ruiz-Capillas, 2020). There is no published data on the rate of physical contamination to meat products in Australian however a recent study from Brazil estimated that the major physical contaminants reported were bone (26.96%), plastic (25.24%) and metal (8.82%).

The Hazard Analysis and Critical Control Points food safety and risk assessment plan developed in the 1960's is a global preventative standard to minimise physical contamination of meat. As a quality assurance, and to ensure no breaks occur in the system, technologies have been developed to check products and detect and isolate any physical contaminants prior to retail (Chen, Zhang, Zhao, & Ouyang, 2013; Edwards, 2004). Chosen detection and removal methodologies vary by foreign bodies size and types, which influence technical realization problems, costs and health consumer's risks. The most common separation techniques are based on the different physical or electrical properties between the intrusion and meat. Detection processes, and any subsequent removal, are systems projected to identify a specific contaminant, based on electronic technologies to simplify it, reducing the costs and to speed up the entire revelation process to make it compatible with production line's speed and imposed reliability parameters (Datta, 2001; Edwards, 2004).

Detection technologies have come a long way, however, low-density foreign bodies such as plastic, wood and fruit stones contaminants are still invisible to established detection systems such as x-ray and infra-red cameras. One technology that may have the potential to determine physical contaminants in meat in a commercial setting is non-invasive microwave imaging technology. Microwave imaging uses low-power, non-ionizing electromagnetic waves, where an antenna transmits and collects back-scattered signals. Microwave signals transmitted into an object can distinguish different components based on their individual permittivity (ϵr) and conductivity (σ), known as dielectric properties. Biological tissues (bone, fat, muscle) have a high contrast in their dielectric properties, allowing for microwave frequencies to distinguish between different tissue layers (Marimuthu, 2016). The higher the conductivity of a substrate, the less penetration of the microwave signal. Substrates with high water content, such as muscle, will have lower penetration as the signal is heavily attenuated (reduced) by the water. Fat and plastic have an oily composition, thus the signal will be less attenuated, resulting in a smaller conductivity and greater penetration. There is a high contrast between the dielectric properties of various low-density materials such as plastics, wood and meat, enabling microwave to distinguish between them. Microwave imaging captures measurements instantaneously and causes no damage to biological tissues, thus can be safely used without shielding in a commercial environment.

Given the high dielectric contrast, we hypothesised that microwave array scanning will be able to detect plastic foreign bodies within meat.

2. Objectives

The objective of these studies were:

- Design, fabricate and test the proposed antenna for detecting foreign objects/material such as plastic in a meat phantom – successfully achieved
- Develop a Microwave Imaging System with array and data acquisition system – successfully achieved
- Develop the proposed confocal imaging algorithm to test the ability to locate plastic objects in a meat phantom – successfully achieved

3. Experiment 1

In this section we detail the proposed the design and development of the microwave imaging system and confocal imaging algorithm to detect different size of plastic in various configurations embedded within a meat and fat phantom to simulate boxed beef trim.

3.1 Antenna Design

This section focuses on the design and development of the most important component in microwave imaging systems: the antenna. The main challenges facing the design of a suitable antenna for imaging systems are the requirements for compact size, moderate to high gain with high radiation efficiency, minimal distortion performance in the time domain, high dynamic range and low profile. Different types of antennas are reported in the literature by researchers seeking the best performance, low profile, reasonable directivity, compact size and low-cost. Vivaldi patch antennas (VPAs) are popular candidates for achieving these requirements (Bourqui, Okoniewski, & Fear, 2007; Langley, Hall, & Newham, 1996) and are widely used in different applications, such as satellite communications, remote sensing, radio telescopes and microwave imaging systems. These kinds of antennas have high directivity, wide bandwidth, simple feed structure, and low cost.

An ultra-wide broadband (UWB) Vivaldi patch antenna was identified, designed and fabricated as shown in Fig. 1 with centre frequency 3.0GHz with bandwidth of 5GHz. The antenna shows return loss less than -10dB for entire bandwidth from 1.4GHz to 6.5GHz. Fig. 2 shows the performance of the antenna.

Figure 2. Proposed ultra-broadband Vivaldi patch antenna

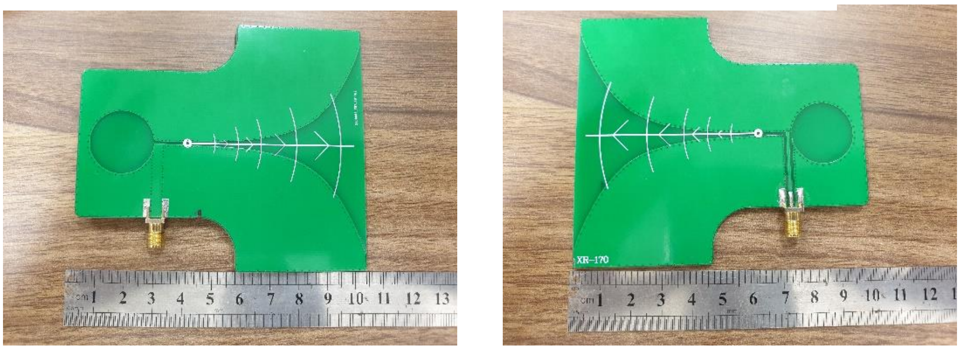

Figure 2. The performance of the proposed antenna a) Magnitude of Return Loss (dB) and b) Phase of Return Loss.

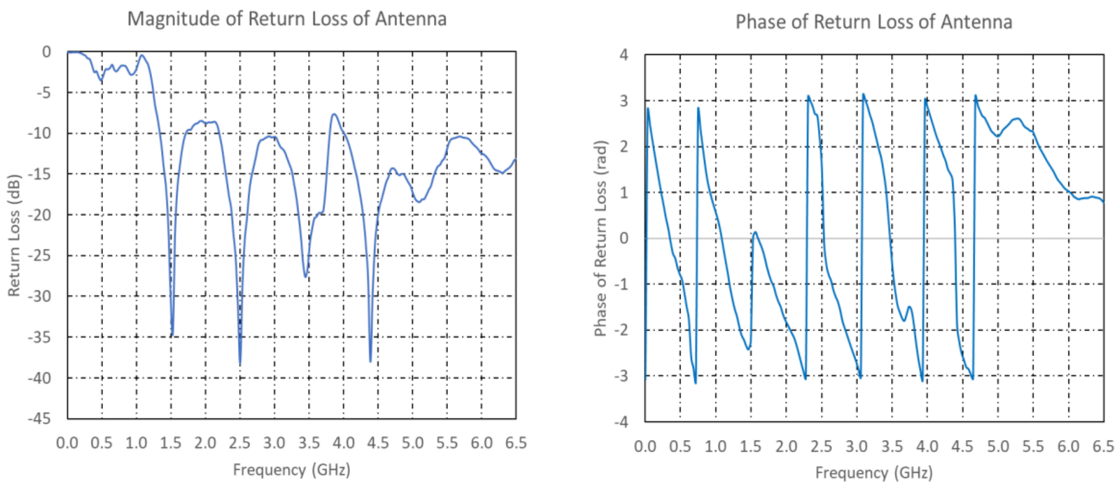

3.2 Microwave Imaging System

A Microwave Imaging System (MIS) with linear array antenna was designed as shown in Fig. 3. The proposed MIS consists of:

a) 4 Vivaldi Patch Antennae
b) Linear Array antenna holder
c) 2 unit of Keysight P9371A (300kHz – 6.5GHz)-4 port Vector Network Analyzer
d) Computer module of OptiPlex 7070 with Python and Matlab with confocal imaging algorithm
e) 4 High quality and phase intolerance microwave cables
f) Meat phantom with plastic

The system has built in automated calibration techniques, data acquisition and confocal imaging algorithm developed in Python and Matlab.

Figure 3. Configuration of the microwave imaging system for plastic detection in meat detection

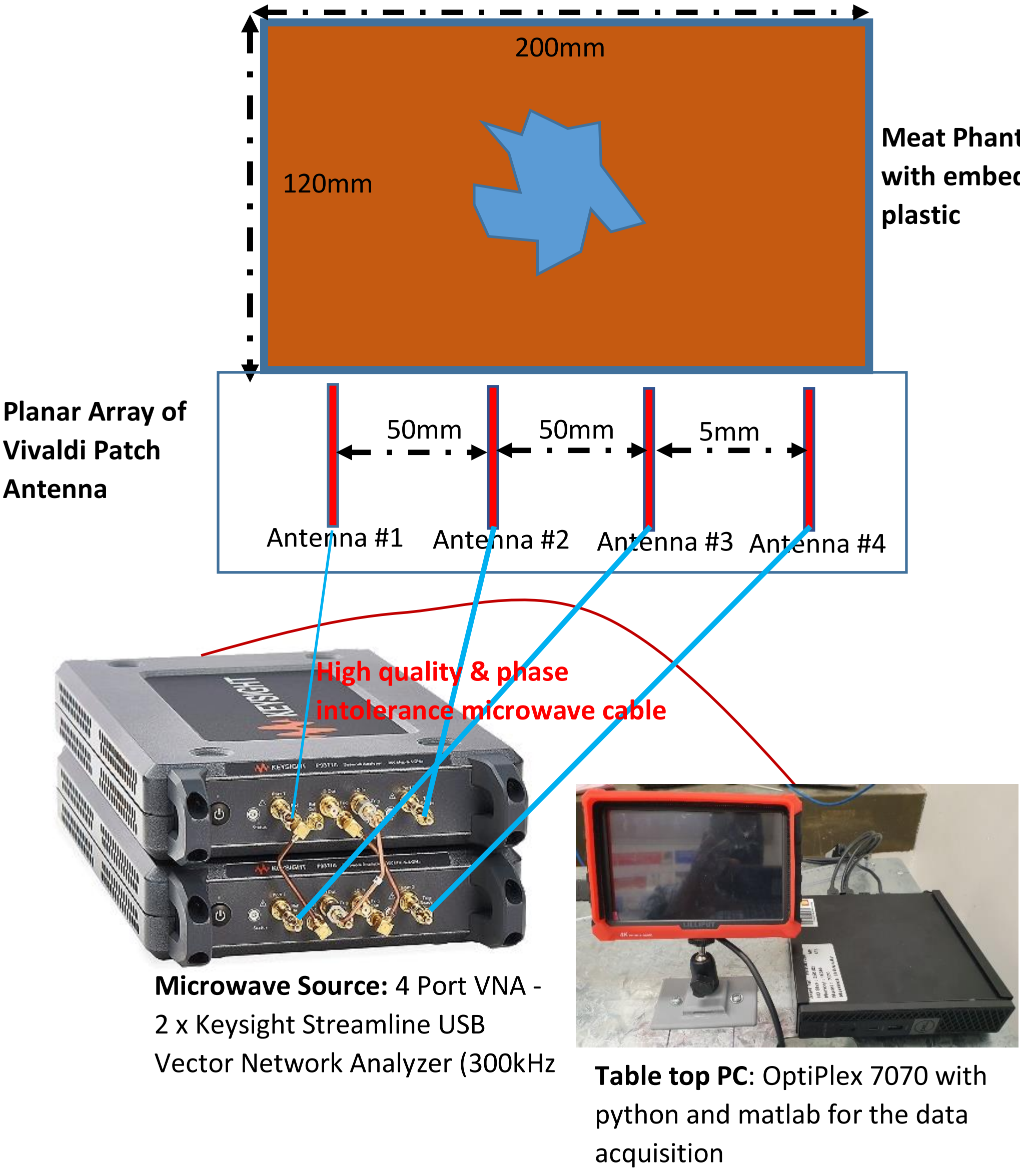

3.2.1 Scanning System Design

Fig. 3 illustrates the configuration of the prototype microwave imaging system comprising the planar array and several other parts, namely, the microwave source, and a personal computer (PC) that was used for the measurements, data storage, processing and image formation. A meat phantom with embedded plastic was used to verify the imaging results of the system. The scanning systems are controlled by Python codes to collect these parameters. The microwave source used in the system was the 2 x Keysight Streamline USB Vector Network Analyzer (VNA) (300kHz – 6.5GHz). In addition, the calibration technique for the VNA ports and the antennas are very important in any successful imaging system. The following section provides the details of the microwave source, the PC and the calibration technique used in the system's measurements. The PC with build in Python and Matlab code has the capability to convert the measured S-parameters from the frequency domain into the time domain for the image reconstruction.

3.2.2 Microwave Source

The microwave imaging system uses the 2 x Keysight Streamline USB Vector Network Analyzer (VNA) (300kHz – 6.5GHz) as a source to generate the microwave signals. It operates from 300kHz to 6.5GHz frequency range. The proposed system has 4-port VNA and is designed to ensure high sensitivity and a wide dynamic range (115dB) over the entire range up to 6.5GHz using a fundamental mixing concept. The proposed system features good bandwidths for this application and extremely fast synthesisers allowing for short measurement times and, thus, provides high throughput in manual adjustments and automated production sequences. The VNA is capable of fast continuous measurement, with less than 3.5ms per measurement. For a typical frequency sweep of 201 points, the total measurement time will be less than 14ms. Due to the analyser's wide dynamic range and low phase noise, this speed advantage does not compromise measurement accuracy. In addition to the manual calibration using the three standards, the VNA can also be calibrated automatically using Keysight electronics calibration unit, which is fast, has low error, and is highly precise compared to the manual calibration. In addition, the VNA provides a reconfigurable firmware that can be remotely controlled by PC facilities for the measurement and data transfer.

3.2.3 Personal Computer

In the proposed imaging system, a PC plays an essential role in the synchronisation, data acquisition and image formation. It was used to control the mode of the operation of the system as follows:

1. With Python code, the PC sends a start signal to the VNA and allows the VNA to be remotely controlled.
2. The Python code remotely sets up the system for the multiple antenna operation, data acquisition and auto calibration of the microwave system by using the Keysight electronics calibration unit.
3. The automated Python code then allows the measurement data for the corresponding set of antennas to be saved on the PC.
4. Steps 1–3 are repeated to allow the second port of the VNA to send the signal to collect the measurement data from another corresponding set of antennas and save the data on the PC.
5. Data calibration and image formation of the phantom was then formulated.

3.2.4 VNA Calibration Technique

To test the imaging system and verify its accuracy in measurement and data collection, a calibration technique involving the measurement of three known standards, namely, the open-circuit, short-circuit and matched load standards, was used. The results allow the three major sources of error during the measurements to be characterised. The proposed calibration techniques reduce system-induced errors significantly. This was achieved by measuring the magnitude and phase response of one or more of these high-quality standards. The standards are placed one at a time where the device under test would normally be at the end of a certain cable. This eliminates errors caused by the cable and its associated connectors. This location is called the "test port". To test the array elements and compare the measured results with the simulation, the VNA was calibrated using the calibration technique as detailed by Pozar (2005).

3.2.5 Planar Antenna Array Design

The first step was to simulate the proposed design in CST Microwave Studio software. A planar antenna array structure was used, comprising of 4 x 1 Vivaldi patch antennas (Fig. 4). In the simulation, the antenna elements are supported by a plastic sheet that has a dielectric constant equal to 3.1.

Two simulations were run.

1) Array structure only to test the optimum distance between antenna for lowest mutual coupling.

   Various formations of antenna placement were conducted, aimed at using the available space most efficiently to fit the proposed phantom size and to avoid mutual coupling between the array elements. Mutual coupling is the communication between two antennas. This communication is unwanted and should be as low as possible (<20 dB).

   The simulation demonstrated the effectiveness of this array as measured by two parameters: the return loss of each antenna was < 10 dB, and the level of mutual coupling between the different antennas was <20 dB.

   The optimum horizontal space between the antenna (hs) at a distance of 50 mm, assuming the array is in free space and in front of the meat phantom with plastic.

Figure 4. The proposed and optimized antenna holder for the planar array system

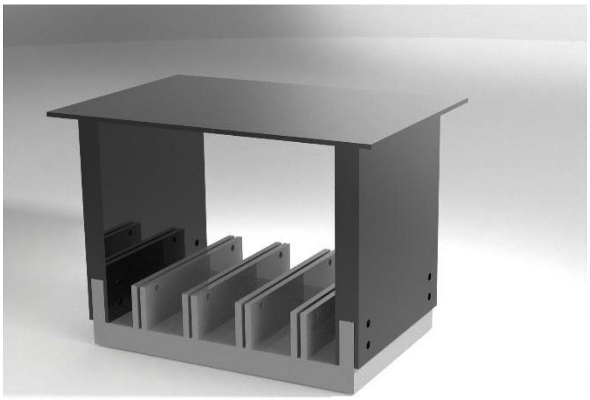

2) Array structure with meat phantom

A model of a meat phantom was created in CST consisting of a plastic container of wall thickness of 2mm, muscle width of 200mm, 100mm depth and 120mm of height embedded with plastic of 50mm diameter at the centre of phantom.

The simulation again demonstrated the effectiveness of the array structure with the meat phantom, with mutual coupling less than -20 dB.

3.2.6 Array and Platform Fabrication

Based on the results from the simulation detailed in section 3.2.5, the microwave planar array system was constructed and fabricated using four Vivaldi patch antenna within a rigid plastic casing (Fig. 5). Each antenna was 110mm long and 80mm wide (Fig. 1).

Figure 5. The fabricated antenna holder with proposed antenna for the planar array system

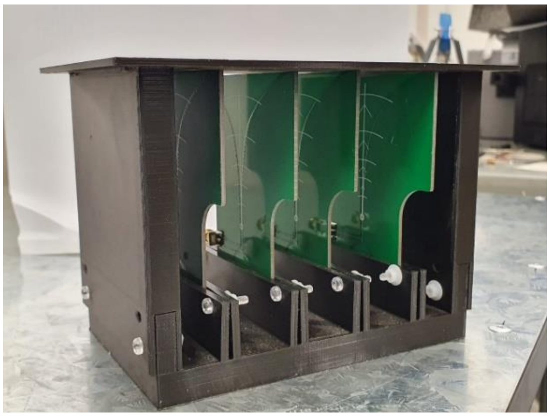

To confirm the performance, the array was tested experimentally. The test was performed with the platform placed in free space prior to scanning of the meat phantoms. The test was successful, demonstrating no issues with mutual coupling between any pair of antennas (less than -25 dB across the band from 3.1 to 10.6 GHz). The level of the measured mutual coupling between any pair of antennas was compared with the level of the simulated mutual coupling.

3.2.7 Experimental setup for boxed beef scanning

Fig. 6 shows the experimental setup of the microwave imaging system. Prior to imaging, the VNA was calibrated as previously described (Section 3.2.4) using three broad coaxial standards (short-circuit, open circuit and matched load standards). However, this calibration does not consider the non-ideal performance of a UWB antenna. Therefore, a modified calibration is performed for the array elements to reduce the effect of the internal reflections of an antenna, as detailed in Section 3.2.9.

Figure 6: Configuration of the microwave imaging system for plastic detection in meat phantom

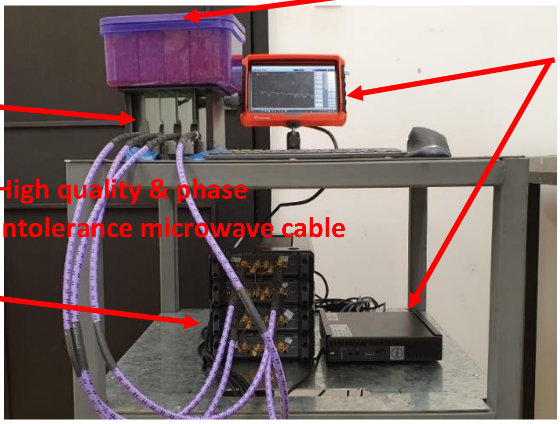

3.2.8 Meat phantom construction

The contrast between plastic contaminants and carcase tissues are likely to be reduced when the fat content is higher. On this basis, three different phantoms were constructed, varying in their muscle to fat ratio. In each case a plastic container of dimension 200mm in width, 100mm depth and 120mm height was used as a mould.

a) Phantom A: 100% minced beef (High contrast)
b) Phantom B: 80% minced beef and 20% fat (Medium contrast)
c) Phantom C: 60% minced beef and 40% fat (Low contrast)

The dielectric properties of these phantoms are shown in Fig. 7 (a) & (b) and Table 1, demonstrating clear differences in their permittivity and conductivity, and thus resulting contrast. A higher permittivity results in a higher contrast, thus easier detection of plastic. However, high conductivity will impede microwave signal penetration, thus the total signal depth achieved will be lower as shown in Fig. 8.

Figure 7. a) Electrical Permittivity, and b) Electrical conductivity between various composition of meat-fat samples and plastic.

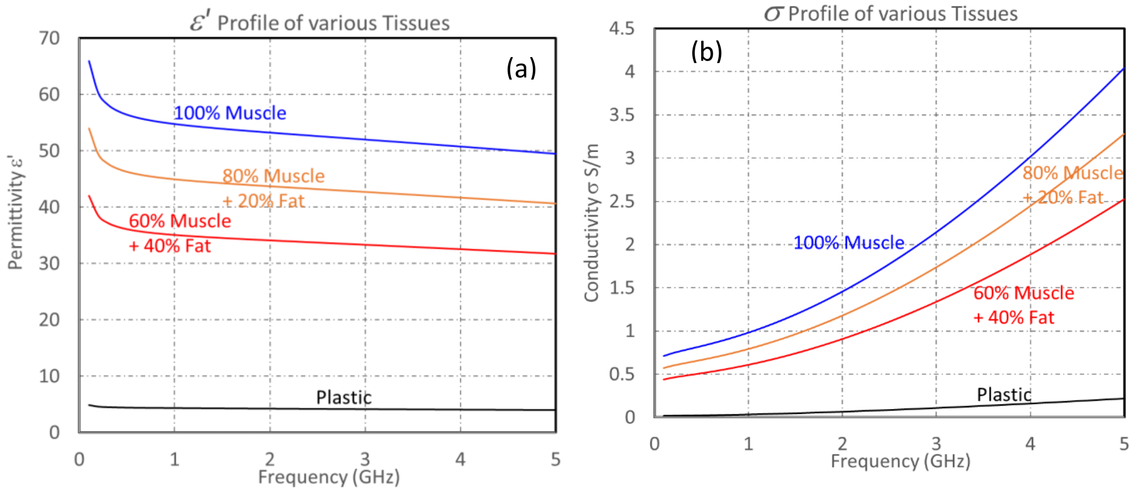

Table 1: Shows the dielectric properties of each designed phantom at 3GHz

	Permittivity at 3GHz	Conductivity at 3GHz	Remarks
Phantom 100% meat	53.0	2.15 S/m	High Contrast Phantom
Phantom 80% meat	44.0	1.75 S/m	Medium Contrast Phantom
Phantom 60% meat	34.5	1.35 S/m	Low Contrast Phantom
Plastic	4.5	0.15 S/m	

Figure 8. Penetration depth for biological tissues.

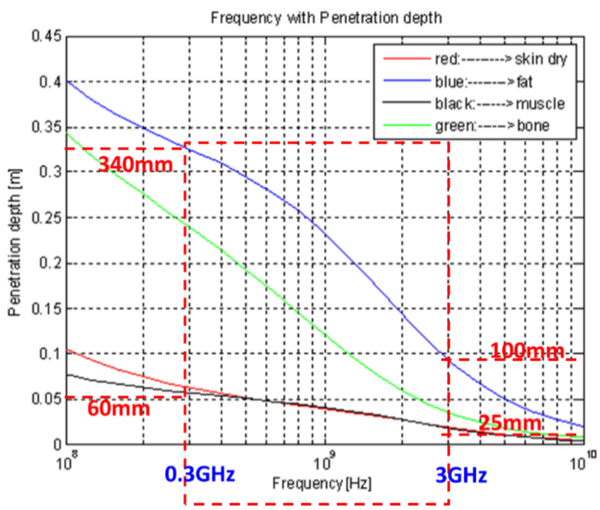

Three different plastic embedding methods were tested within each phantom;

a) Embedding method A: 50mm diameter solid plastic sphere placed in the centre of phantom (approximately 62mm from antenna) as shown below.

Figure 9. Embedding method A

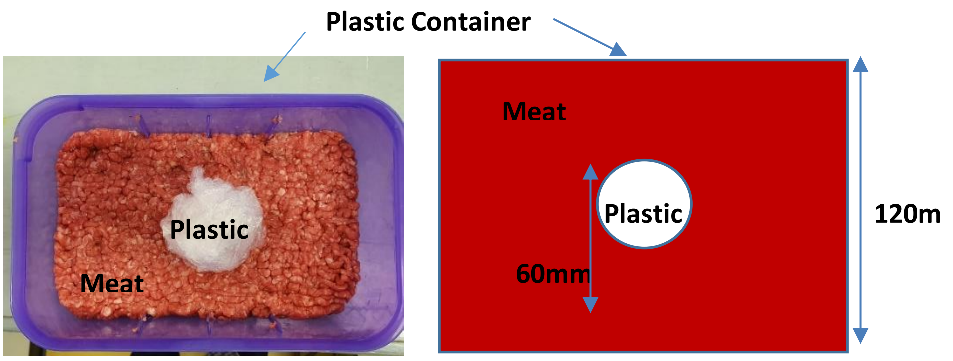

b) Embedding method B: 3x 25 mm diameter solid plastic spheres placed at a 30 mm distance from the antenna

Figure 10. Embedding method B

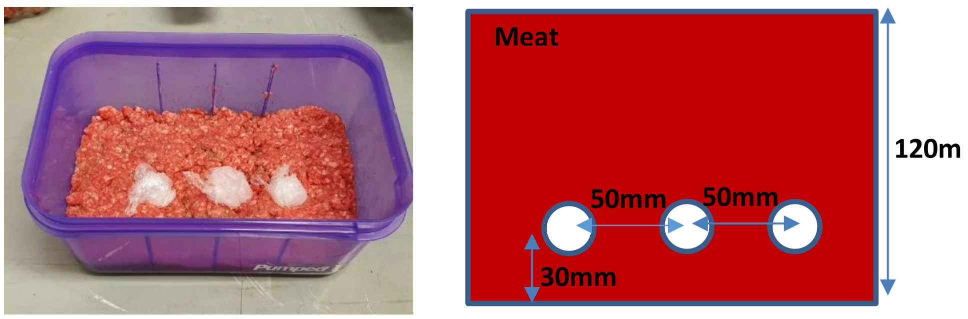

c) Embedding method C: 2mm thick rectangular shaped plastic sheet placed diagonally.

Figure 11. Embedding method C

3.2.9 VNA and Array Element Calibration

The VNA included a probing antenna that must be calibrated to compensate for any non-ideal operation of this apparatus using the standard one-port calibration procedure involving the three broad coaxial standards. To reduce the non-ideal performance of the antenna elements, an error network model like the one used in the VNA one port calibration procedure must be applied. In this case, we need to define a four-port network with single-mode fields at Port #1, Port #2, Port #3 and Port #4 of the VNA. This condition can be readily applied for all ports which are a coaxial input port of the antenna. However, since the antenna are placed within an array, strong mutual coupling can be present due to nearby antennas. When designing the antenna array for this application, steps are taken to ensure that the mutual coupling between antennas is reduced. Due to the strong reflection from the air-meat interface, the reflections coming from neighbouring antennas should be less than -20 dB for better detection of the plastic in the proposed phantoms. With a proposed Vivaldi patch directional antenna design, this is quite feasible. A calibration technique, which uses three standards, was used in this study (Marimuthu, 2016). The proposed calibration technique simultaneously corrects for the systematic error in the cabling and RF frontend, as well as the array errors due to mutual coupling, antenna alignment and manufacturing error. The three standards are free space, water and oil. This technique ensures that the antenna array can be calibrated without removing the individual antennas from the array. The proposed technique can solve the above-listed problems and improve the detection and localisation of the plastic within the proposed phantom.

3.2.10 Data Acquisition

The experimental prototype system shown in Fig. 12 was used in the monostatic mode of operation. The monostatic mode was operated when the 4-antenna element of the planar array are used to image the object. The UWB pulses are generated using the VNA in a step-frequency manner across the band from 1.0GHz to 6.5GHz. The data (complex S-parameters) are collected by activating Port #1 to Port #4 and the PC to record the data from the 4-antenna element of the planar array, S11, S22, S33 or S44 as shown in Fig. 13(a). The monostatic approach was chosen as it has so far given satisfactory results and avoids the complexity in hardware and software required for a multi-static approach. The object (rectangular meat phantom with plastic) was placed on the platform as shown in the Fig. 12.

Figure 12. The detail of array with meat phantom

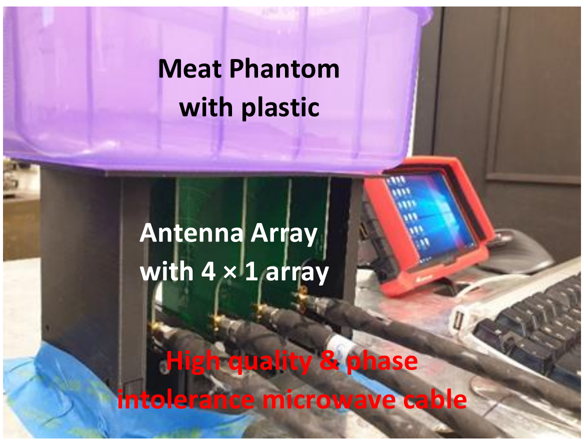

Figure 13. The measured S11, S22, S33 and S44 for 4 antennas in array platform (a) without any phantom, (b) with 100% meat phantom without plastic inside the phantom, and (c) with 100% meat with plastic embedded at position C.

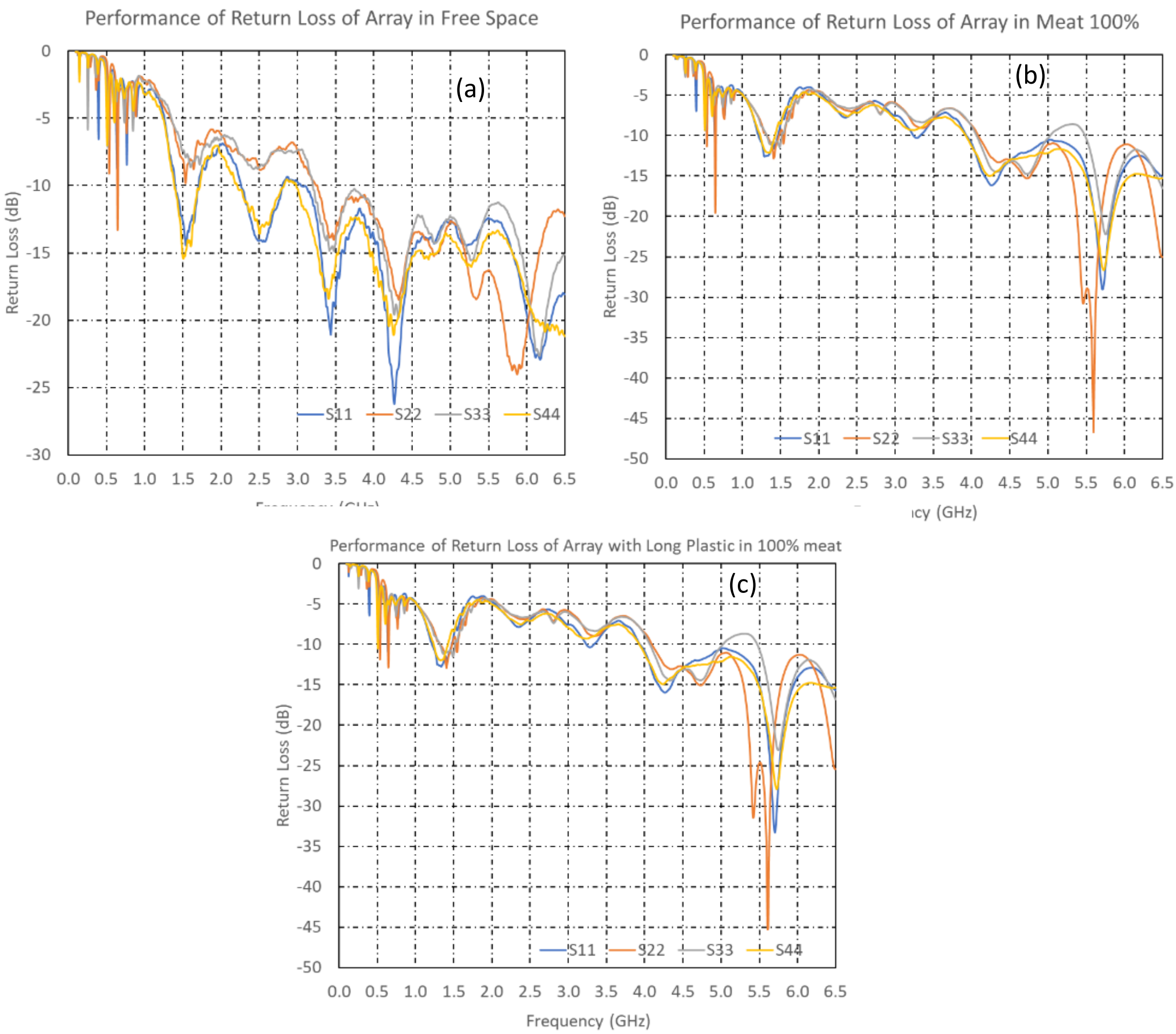

All 4 antenna elements are used as transmitters and receivers. Initial data for the two ports (S11, S22, S33, S44) of the VNA are recorded when there is no imaged object (meat phantom) present in the platform as shown in Fig. 13(a). These data are subsequently used to remove reflections caused by the platform.

The phantom was placed on top of the antenna for measurements. In the data acquisition, initial measurements were taken without any phantom, to record the performance of the antenna in free space while in array platform. Then the experiment was repeated by placing the meat phantoms with plastics in various configurations, depicted in Fig. 13(b) & (c). The time domain analysis is depicted in Fig. 14.

Figure 14. The measured time domain of S11, S22, S33 and S44 for 4 antennas in array platform with 100% meat phantom embedded with plastic configuration C.

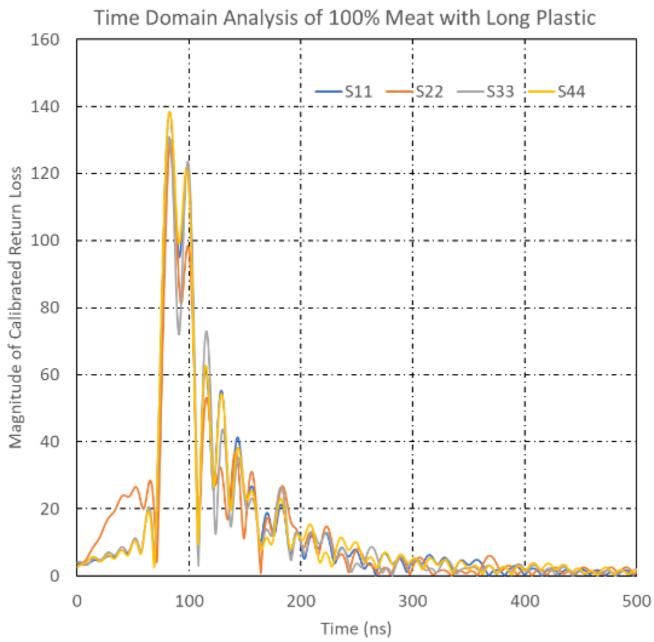

3.3 Microwave Imaging

The four ports of the VNA (Port #1, Port #2, Port #3 and Port #4) were calibrated across the proposed UWB frequency using 3 standards prior to microwave scanning. Following the data collection, a post-processing algorithm was applied to reconstruct the images. A modified delay-and-sum confocal algorithm (Ireland & Bialkowski, 2011) was used to reconstruct the rectangular phantom. To create accurate images, it is necessary to find the correct path on which the wavefront travels. For that reason, Fermat's principle was used to estimate the path of the wave. The principle states that the path resulting in the minimal propagation time is the real path. The electromagnetic signals travel in the coupling medium and the heterogeneous phantom; therefore, the average dielectric properties of the imaged body must be estimated to accurately predict the length of the electrical path of the signal.

The microwave imaging setup data for this system are presented in Fig. 15. The points that lie on the surface of the phantom are denoted by $\boldsymbol{Bi}(\boldsymbol{x}, \boldsymbol{y}, \boldsymbol{z})$. Any discrete point inside the surface is denoted by $\boldsymbol{p}\mathrm{i}(\boldsymbol{x}, \boldsymbol{y}, \boldsymbol{z})$. The phantom permittivity and conductivity are denoted by $\boldsymbol{\epsilon P}$ and $\boldsymbol{\sigma P}$. The medium surrounding the body to be imaged has permittivity and conductivity of like free space. The 4 antenna elements of the planar array are used as signal sources. Before the confocal process can be applied, it is necessary to perform the following pre-processing steps:

Figure 15: Microwave imaging set-up used in the post-processing algorithm

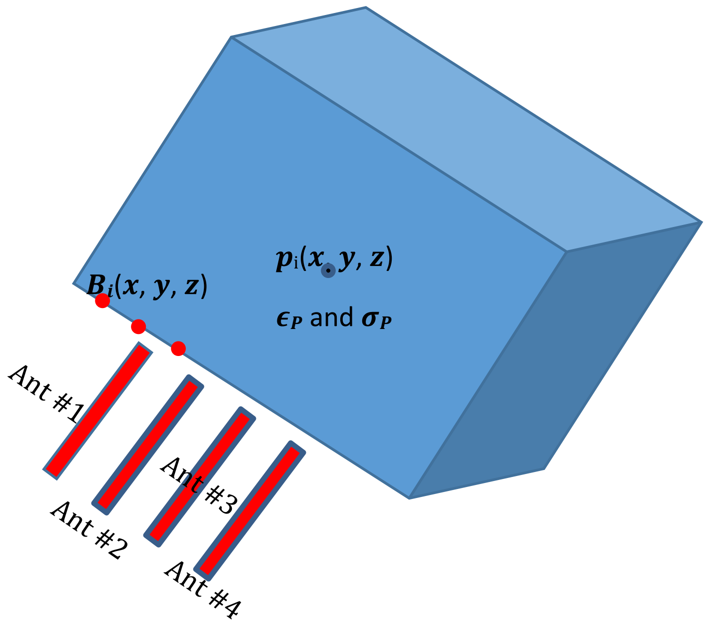

N time-domain signals $A_n(t)$ should be obtained where n = 1, 2, 3, …., N (N=4 in this work). The scattered signals can be obtained from the incident and the total field:

$$\boldsymbol{A_n^{scatter}(t) = A_n^{total}(t) - A_n^{incident}(t)} \quad (1)$$

where n = 1, 2,3, …., N

To cancel any background or surroundings signals such as the reflections from the plastic container wall, array system, the differences in the signals between the antennas are constructed. For n = 1,2, …., $N - 1$:

$$\boldsymbol{F_n(t) = A_n^{scatter} - A_{n+1}^{scatter}} \text{ and } \boldsymbol{F_N(t) = A_N^{scatter} - A_1^{scatter}} \quad (2)$$

To mathematically explain the iterative process of the imaging algorithm, it is convenient to define several mathematical sets. Referring to Fig. 15, we consider the object to be discretised into points denoted by p defined in Euclidean space by (x, y, z) coordinates. Boundary points that exist on the edges of the body to be imaged are denoted as $\boldsymbol{B_d}$ = {$\boldsymbol{B_1}$ $(\boldsymbol{x}, \boldsymbol{y}, \boldsymbol{z})$, $\boldsymbol{B_2}$ $(\boldsymbol{x}, \boldsymbol{y}, \boldsymbol{z})$, $\boldsymbol{B_3}$ $(\boldsymbol{x}, \boldsymbol{y}, \boldsymbol{z})$, ⋯⋯ , $\boldsymbol{B_{Nb}}$ $(\boldsymbol{x}, \boldsymbol{y}, \boldsymbol{z})$ } where $\boldsymbol{B_i}$ $(\boldsymbol{x}, \boldsymbol{y}, \boldsymbol{z})$ is the $\boldsymbol{i}$ boundary points in the rectangular space defined by the x, y and z coordinates, and $\boldsymbol{N_b}$ is the number of boundary points corresponding to the plastic container wall.

The set which contains all the points in the body and on the surface is denoted as Z. The antenna spatial coordinates are denoted as {$\boldsymbol{An} = \boldsymbol{An_1}\,(\boldsymbol{x}, \boldsymbol{y}, \boldsymbol{z})$, $\boldsymbol{An_2}\,(\boldsymbol{x}, \boldsymbol{y}, \boldsymbol{z})$, $\boldsymbol{An_3}\,(\boldsymbol{x}, \boldsymbol{y}, \boldsymbol{z})$, $\cdots\cdots$, $\boldsymbol{An_N}(\boldsymbol{x}, \boldsymbol{y}, \boldsymbol{z})$ } where $\boldsymbol{An_i}\,(\boldsymbol{x}, \boldsymbol{y}, \boldsymbol{z})$ is the $\boldsymbol{ith}$ antenna and $\boldsymbol{N}$ is the number of antennas. The elements array is denoted by $\boldsymbol{An}\mathrm{t}_1$, $\boldsymbol{An}\mathrm{t}_2$ …., $\boldsymbol{An}\mathrm{t}_4$.

The pseudo-code for the confocal imaging algorithm is:

```
begin
    for n ← 1 to N do
        for ∀p ∈ Z do
            for d ← 1 to N_b do
                D_d ← √ε_m ||An_n − B_d|| + √ε_ph ||p − B_d||
            D ← min {D_1, D_2, ..., D_{N_b}}
            τ ← [2 × D/c]
            I(p) ← I(p) + F_n(τ)
```

Here we implement Fermat's principle by constructing all the possible propagation paths from the antenna to the boundary points, and then from the boundary points to the current point p in the image domain; accordingly, our optimal path is the minimal electrical distance. We then obtain the time delay according to the distance and the velocity of the wave in the free space prior to the image domain and in the phantom. A continuous colour image is produced using a shading operator to interpolate at the non-tested points. Strong intensity colours indicate the location of significant scattering objects, such as plastic. The average value of the permittivity and the conductivity for the meat phantom are set at ϵ_{ph} = 48 and σ_{ph} = 1.5, respectively. The algorithm provides the iterative process to construct the image from the processed scattered data. The colour map intensity, denoted by I, is given as a function of p.

To evaluate the effectiveness of the produced images, quantitative metrics are used (Ireland & Bialkowski, 2011). To explain the metrics used, it is convenient to define a further set of points $\boldsymbol{\mathcal{T}}$ that map the location of the plastic in the meat phantom. The first metric is the ratio of the average intensity value of points located in the plastic area, divided by the average intensity points in the normal meat tissues denoted as Q and defined as:

$$\boldsymbol{Q} = \frac{\mu[\boldsymbol{I}\,(\boldsymbol{p})]\ \ \forall \boldsymbol{p} \in \boldsymbol{\mathcal{T}}}{\mu[\boldsymbol{I}(\boldsymbol{p})]\ \ \forall \boldsymbol{p} \notin \boldsymbol{\mathcal{T}}} \tag{3}$$

where $\mu[\bullet]$ is the mean function. A higher value for this metric means the intensity of the plastic region is larger than the intensity of the background regions. The second metric represents the ratio of the maximum intensity value of the plastic area over the maximum intensity of the remaining points in the colour map, denoted by γ, and given as:

$$\gamma = \frac{\boldsymbol{max}[\boldsymbol{I}(\boldsymbol{p})] \;\; \forall \boldsymbol{p} \in \mathcal{T}}{\mathbf{max}[\mathbf{I}(\mathbf{p})] \;\; \forall \boldsymbol{p} \notin \mathbf{Z}} \qquad (4)$$

The third metric is the absolute distance between the location of the plastic and the location of the point with the maximum intensity given in the reconstructed image. If (**t**) denotes the centre of the plastic, this metric is defined as follows:

where:

$$\boldsymbol{p}^{*} = \frac{\boldsymbol{argmax}[\boldsymbol{I}(\boldsymbol{p})]}{for\ \mathbf{p} \in \mathcal{T}} \qquad (5)$$

3.4 Results

The images below represent the scanning of;

- 100% meat phantom, no plastic (Fig. 16)
- 100% meat phantom, with plastics in configuration A, B & C (Fig. 17)
- 80% meat phantom, with plastics in configuration A, B & C (Fig. 18)
- 60% meat phantom, with plastics in configuration A, B & C (Fig. 19)

Within these images a colour scale is applied, representing substrate permittivity. Blue indicates high permittivity and yellow low permittivity.

In Fig. 16 where no plastic contaminants were embedded an area of reduced permittivity appears at the surface of the phantom, likely indicating high reflection due to air-meat interface.

Figure 16. Phantom with 100% meat without any embedded plastic.

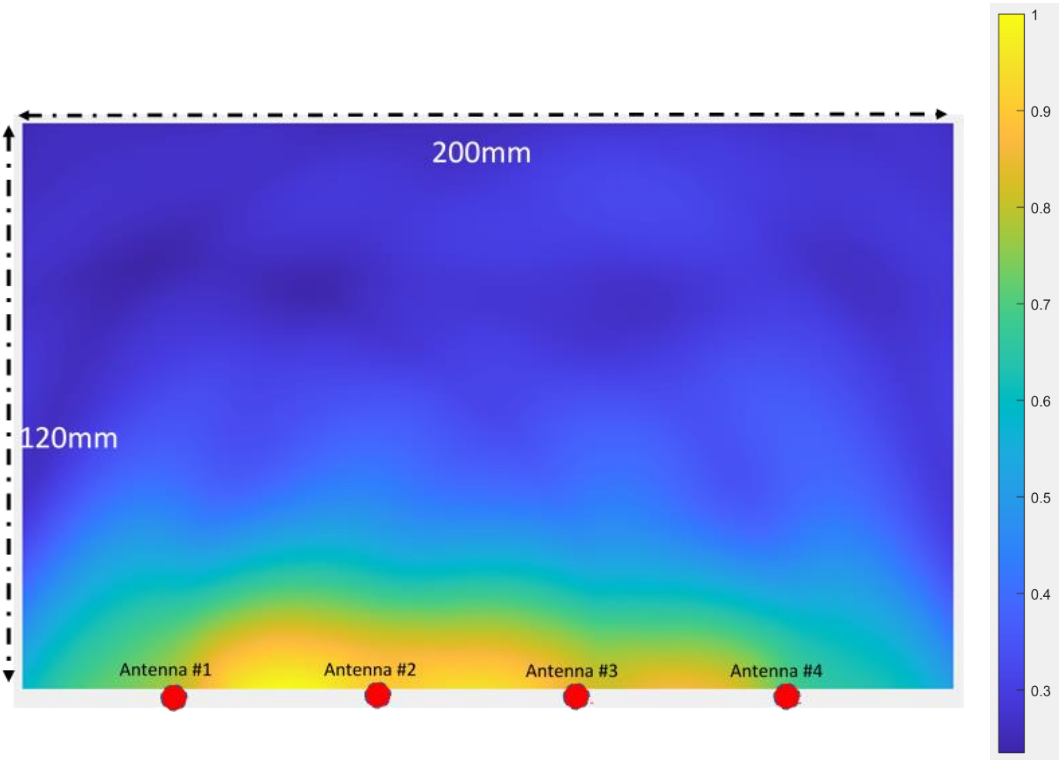

Fig. 17 (a) and (b) have focal yellow points within the image corresponding to the embedded plastic. The three clearly defined yellow focal points in Fig. 17 (b) demonstrates the ability to successfully detect multiple small plastic contaminants. Fig. 17 (c) is less well defined indicating that the microwave may not be able to penetrate to that depth due to the conductivity of the substrate.

In all three images, significant shadowing is present indicating some inefficiency in object identification. The air-meat interface is not as visible in Fig. 17 (a), (b), & (c) because of the presence of plastics within the phantom so the background noise will be suppressed.

Figure 17. Array of antenna (4 antennas) with 100% meat and (a) 50mm diameter of plastic at centre (b) Three 25mm of plastic (c) Rectangular shaped 2mm thick plastic placed diagonally in meat phantom.

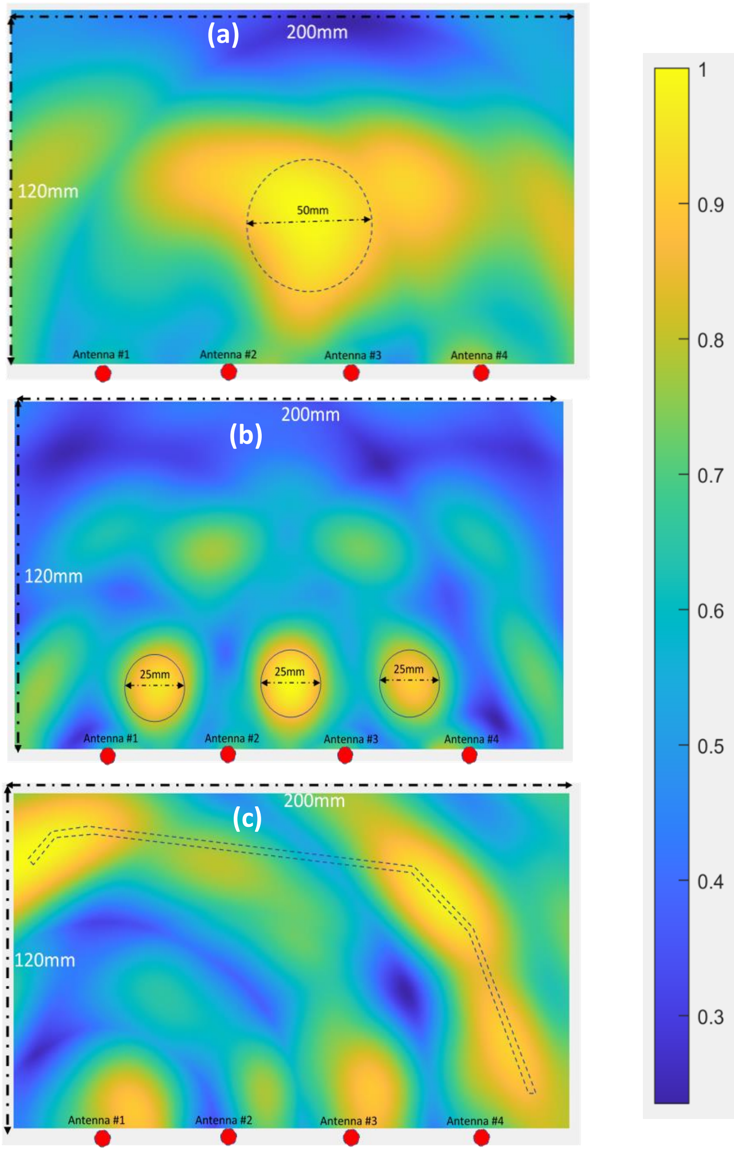

In Fig. 18, the plastics have been identified with a similar level of specificity as shown in Fig. 17. The shadowing was slightly greater than Fig. 17 with less well defined structures, due to the lower conductivity of the medium.

Figure 18. Array of antenna (4 antennas) with 80:20 meat:fat ratio and (a) 50mm diameter of plastic at centre (b) Three 25mm of plastic (c) Rectangular shaped 2mm thick plastic placed diagonally in meat phantom.

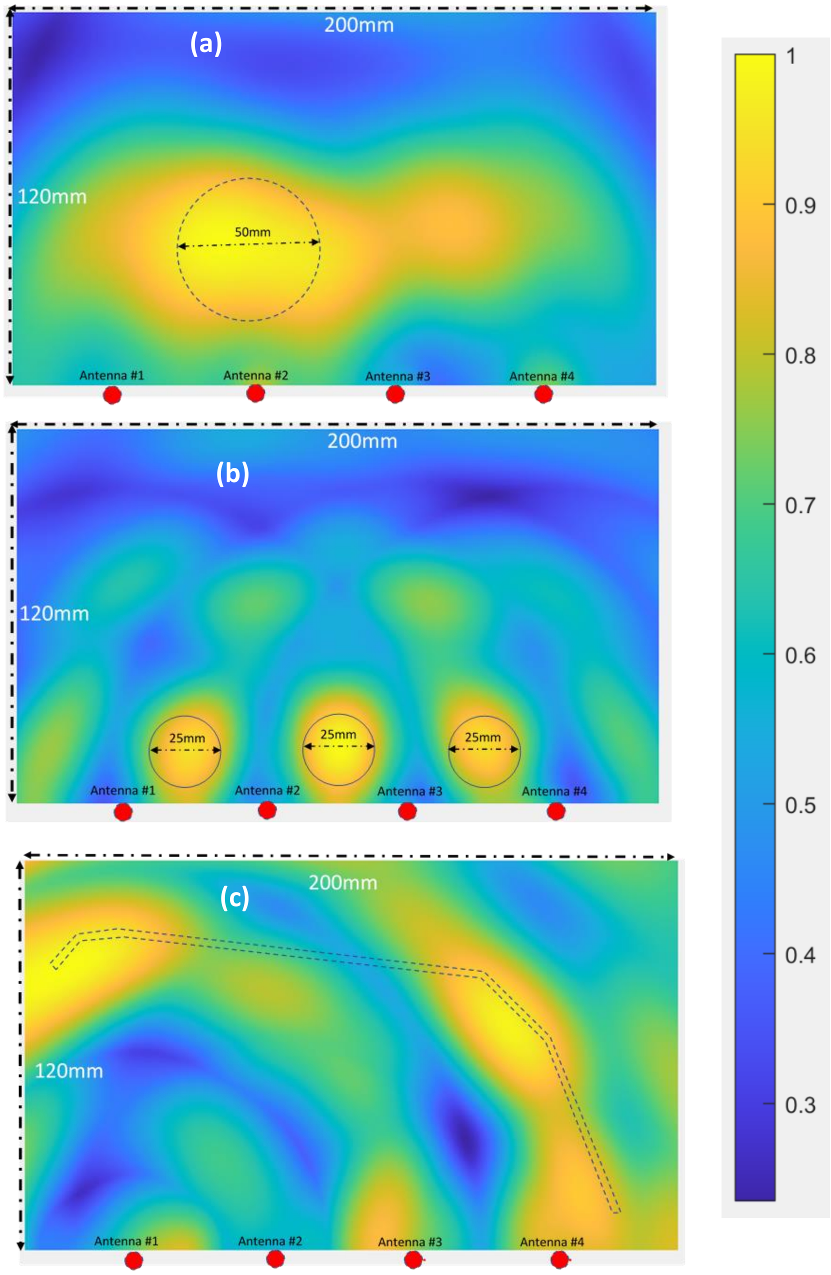

Fig. 19 demonstrated the testing of the lowest meat and highest fat content, thus the plastic to tissue contrast was minimised. The imaging was still visually able to perform at a similar level to Fig. 17 and 18.

Figure 19: Array of antenna (4 antennas) with 60:40 meat:fat ratio and (a) 50mm diameter of plastic at centre (b) Three 25mm of plastic (c) Rectangular shaped 2mm thick plastic placed diagonally in meat phantom.

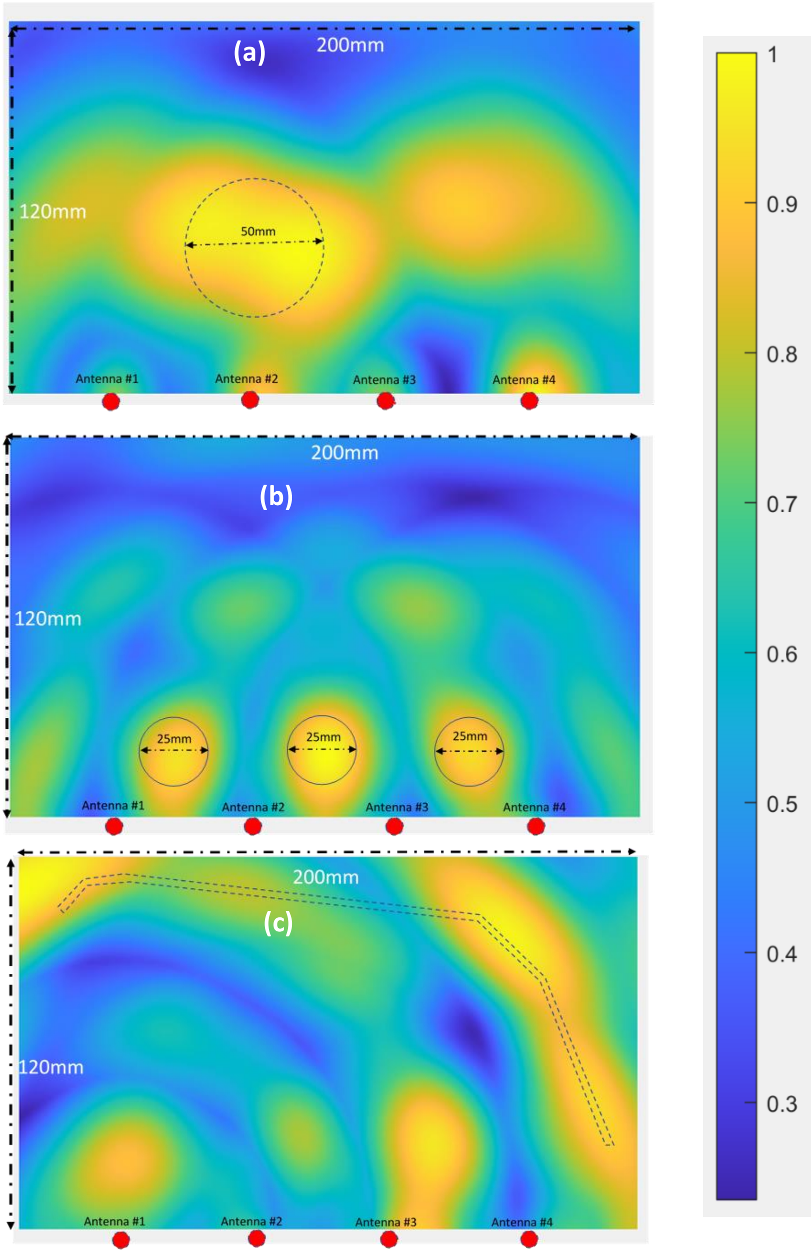

3.5 Conclusion and Discussion

The results demonstrate a crude ability of the proposed UWB microwave imaging system to detect and localise plastic contaminants within cartons of meat trim containing between 60 – 95% chemical lean. However, considerable image artefact exist suggesting the need to improve both the hardware and analytical approach deployed in this experiment.

The potential limitations in our hardware design were as follows.

- The confocal imaging used the return loss (S11, S22, S33 and S44) signals only from the antennas in the array.

Potential limitations in our analytical design were as follows.

- The confocal imaging used a delay-sum algorithm which required the return loss signals in the frequency domain to be convert to time domain signals. The performance of the system to image the plastic with four antennas can be further improved by using more sophisticated imaging algorithms such as Truncated Singular Value Decomposition (TSVD) which not only uses the return loss (S11, S22, S33 and S44) but also insertion loss signals (S12, S13, S14, S21, S23, S24, S31, S32, S34, S41, S41, and S43) (Gilmore, Mojabi, Zakaria, Ostadrahimi, Kaye, Noghanian, Shafai, Pistorius, & LoVetri, 2009). The TSVD can be developed based on frequency domain signals by using single frequency or multiple frequencies. This technique will also eliminate unnecessary images or shadowing present in confocal imaging as shown in Fig. 7 – 19.

Potential next steps

1) Develop image algorithm based on TSVD, using all 16 signals within the frequency domain. This will potentially improve image quality, localisation, shape and capacity to identify the type of a physical contaminant.
2) Increase the number of antennas from 4 to 8 or 16. This will improve the location precision as well as the resolution between multiple targets.
3) A new calibration technique for the array will also be tested using three standards. The calibration technique simultaneously corrects for the systematic error in the cabling and RF frontend, as well as the array errors due to mutual coupling, antenna alignment and manufacturing error. The proposed three standards are free space, water and oil. The technique ensures that the antenna array can be calibrated without removing the individual antennas from the array. The proposed technique can solve the above-listed problems and improve the detection and localisation of the plastic or an unwanted object within the meat under test.
4) Develop an industry-suitable food-grade conveyor system. The proposed conveyor system has a multiple speed controller and the capacity to integrate all sixteen antennas. Fig. 20 and 21 depict the proposed conveyor-microwave imaging system.

Figure 20. Complete industrial based automated microwave imaging system with sixteen antennas on food grade conveyor system for multiple and automated real imaging of the meat for plastic or unwanted object detection.

Figure 21. Shows various parts of the completed system of industrial based automated microwave imaging system with sixteen antennas on a food grade conveyor system.

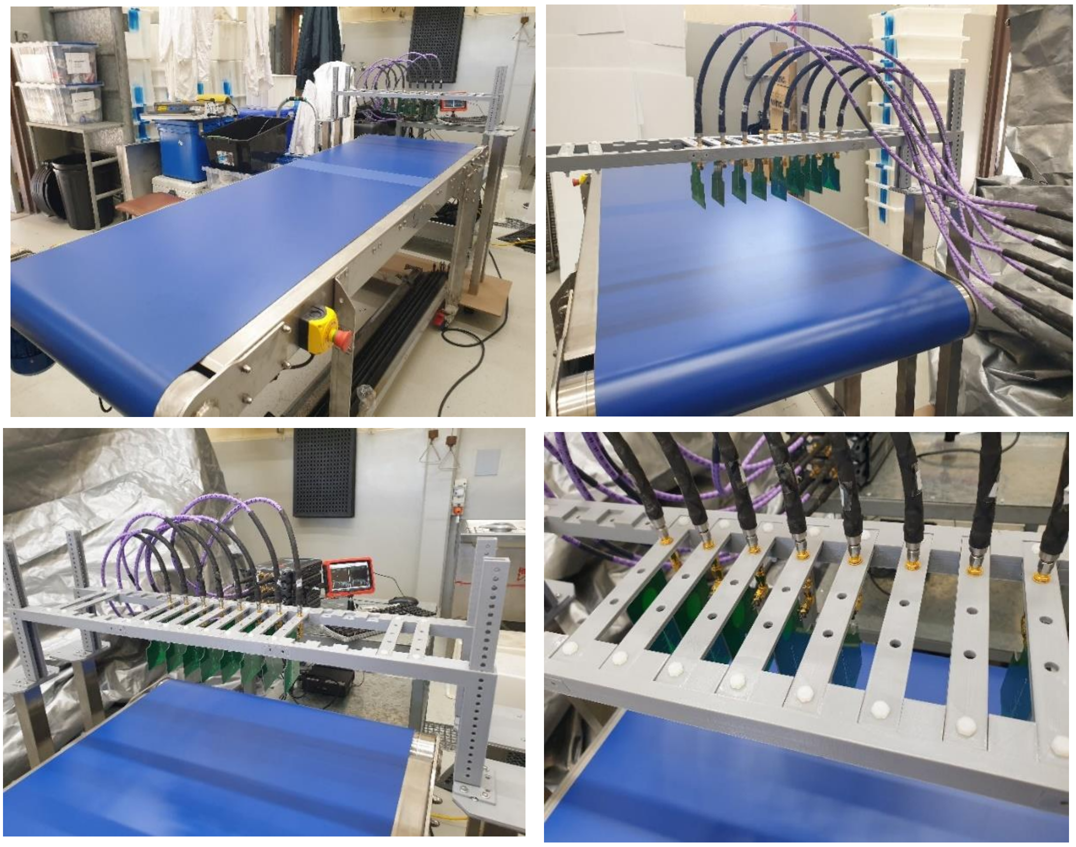

4 Experiment Two

The aim of Experiment 2 was to design and develop a microwave imaging system to detect different sized plastic in chunks of beef on a conveyor belt.

4.1 Antenna Design

Two antennas were tested in Experiment Two. The first antenna was the Vivaldi Patch Antenna detailed in Section 3.1 above.

The second antenna was a wide broadband Horn antenna, depicted in Fig. 22. The Horn antenna has a centre frequency 5.5GHz with bandwidth of 4GHz. The antenna shows return loss less than -10dB for the entire bandwidth from 3.5GHz to 7.5GHz. The performance of the antenna is depicted in Fig. 23.

Figure 22. Broadband Horn antenna

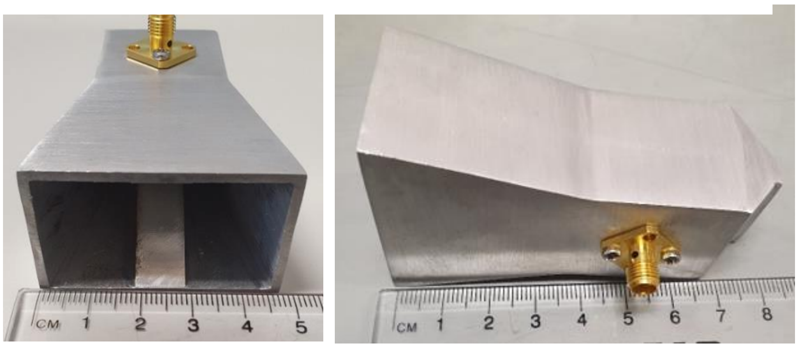

Figure 23. The performance of the proposed antenna (a) Magnitude of Return Loss (dB) and (b) Phase of Return Loss.

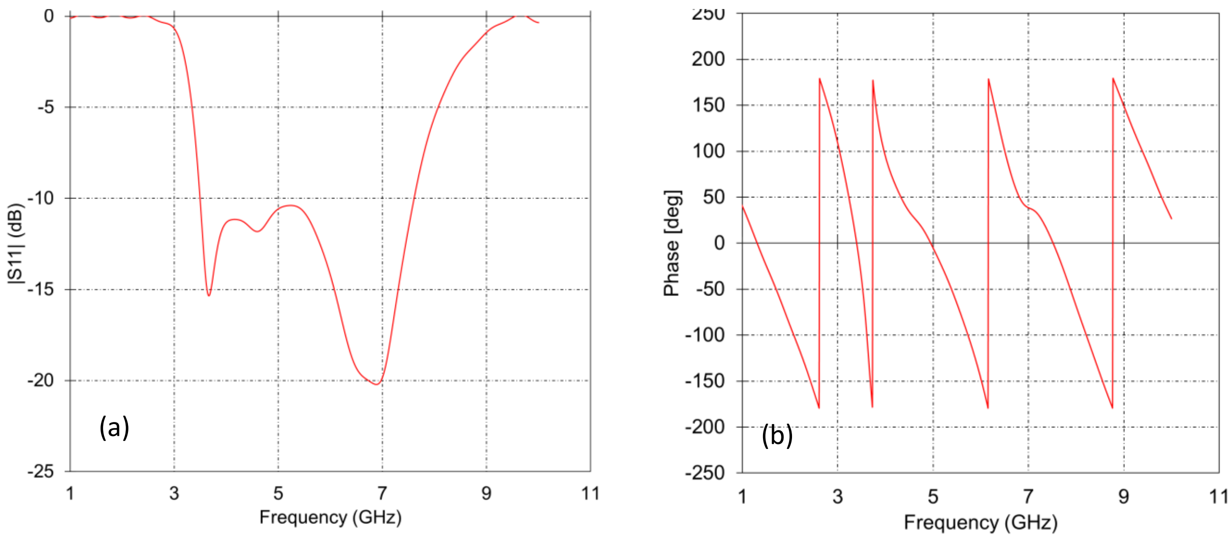

4.2 Microwave Imaging System

An automated microwave imaging system with a linear array antenna configuration unit was designed as depicted in Fig. 24 and 25. The components included:

a) 8 Vivaldi Patch antennas and 8 horn antennas

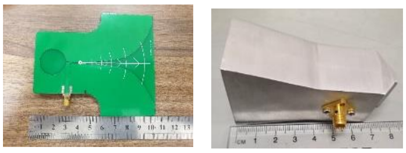

b) 18 antenna unit linearly configured (design for mounting Vivaldi patch antenna and horn antenna)

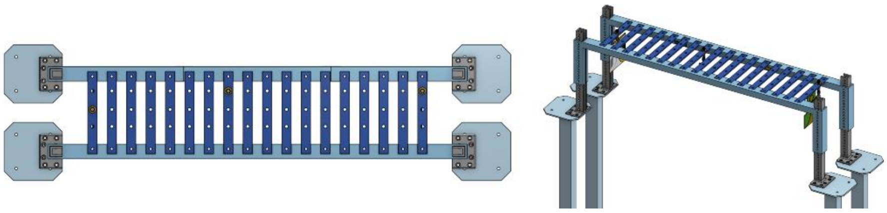

c) Food grade speed adjustable industrial conveyor system

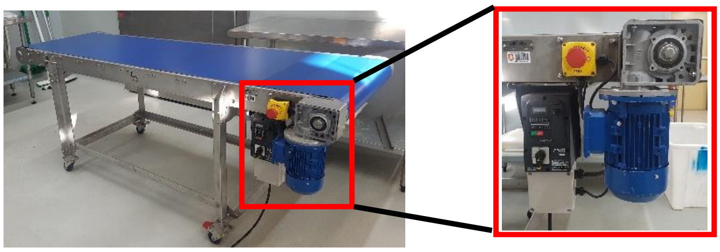

d) 4 units of Keysight P9371A (300kHz – 6.5GHz) – eight (8) port Vector Network Analyzer

e) Computer module of OptiPlex 7070 with Python and Matlab with confocal imaging algorithm

f) 8 units of high quality and phase tolerance microwave cable

g) Various meat phantoms with and without plastic

The system has built with automated calibration techniques, conveyor speed control, and data acquisition developed in Python.

Figure 24. Complete industrial based automated microwave imaging system with eight (8) Vivaldi Patch antennas on food grade conveyor system for multiple and automated real imaging of the meat for plastic or unwanted object detection.

Figure 25. Shows various part of the completed system of industrial based automated microwave imaging system with sixteen antennas on food graded conveyor system

4.3 Scanning System Design

Fig. 24 and 25 illustrate the configuration of the proposed microwave imaging system, which is automated and mounted on a conveyor. This system comprised of;

- linearly configurable planar array unit for eighteen (18) antenna (designed for mounting Vivaldi patch antenna or horn antenna),
- food grade speed adjustable industrial conveyor system
- microwave source (4 unit of Keysight P9371A (300kHz – 6.5GHz) eight (8) port Vector Network Analyzer), and a personal computer (PC) that was used for the control of conveyor system, microwave scanning, data storage, processing and image formation.

The proposed system has the capacity to capture multiple scans based on defined timing steps that are in line with the speed of the conveyor system. The conveyor system has a specific scanning area of size 1124mm x 594mm with a Teflon base (Fig. 26). The whole microwave scanning unit with the array of antenna will be placed on top of the Teflon based scanning area as shown in Fig. 25.

A meat phantom with embedded plastic was used to verify the imaging results of the proposed system as shown in Fig. 27. The scanning area for horn antenna-based array (with 8 antennas) is 60cm wide. The scanning area for Vivaldi patch antenna (with 8 antennas) is 40cm wide. The scanning systems are controlled by Python code based on speed of the conveyor systems. In this experiment the conveyor system was set at 4.3cm/s speed with scanning of 13 measurements for 13.75s. Meaning for every 4cm, one microwave scanning via eight antennas is performed.

The microwave source used in the system was the 4 x Keysight Streamline USB Vector Network Analyzer (VNA) (300kHz – 6.5GHz). In addition, the calibration technique for the VNA ports and the antennas are very important in any successful imaging system. The following section provides the details of the microwave source, the PC and the calibration technique used in the system's measurements. The PC with build in Python and Matlab code has the capability to convert the measured S-parameters from the frequency domain into the time domain for the image reconstruction.

Figure 26. The conveyor system scanning area.

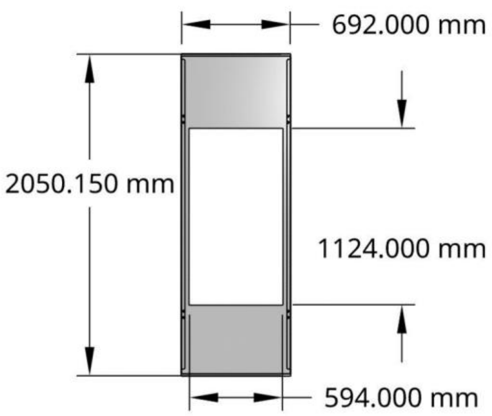

4.4 Experimental set up for loose beef scanning

The experimental set-up of the microwave imaging system with array of antennas is depicted in Fig. 27. Prior to imaging, the VNA was calibrated as previously described (Section 3.2.4) using three broad coaxial standards (short-circuit, open circuit and matched load standards). However, this calibration does not consider the non-ideal performance of a wideband antenna. Therefore, a modified calibration is performed for the array elements to reduce the effect of the internal reflections of an antenna, as detailed in Section 3.2.9.

Two different configurations of meat phantoms were scanned as detailed in Section 4.5

Figure 27. (a) Horn antenna array system, and (b) Vivaldi patch antenna array system with meat samples and visible plastics.

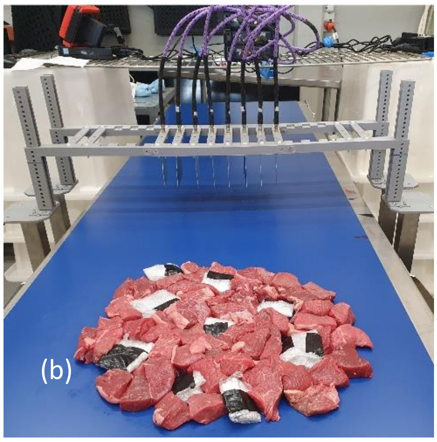

4.5 Meat Phantom construction

Two phantoms designs were constructed.

4.5.1 Phantom 1. Visible Plastic

Phantom 1 tested the ability of the microwave system to detect visible plastics within trimmed beef meat samples on a moving conveyor system as depicted in Fig. 28.

Figure 28. Phantom 1 designed using trimmed beef meat samples with visible plastic on a conveyor system at various scanning positions by using an array of antenna on an automated conveyor system using (a) horn antenna and (b) vivaldi patch antenna array.

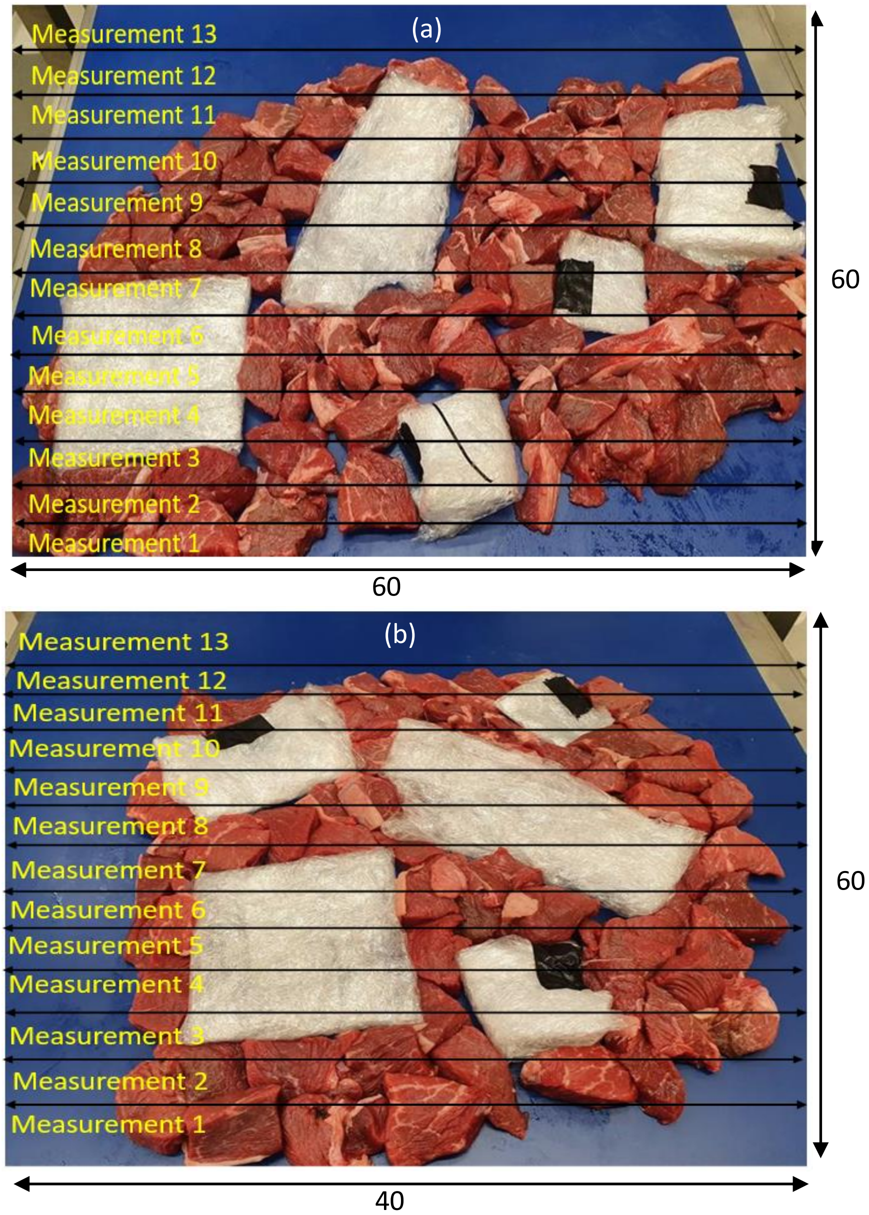

4.5.2 Phantom 2. Non-visible Plastic

Phantom 2 tested the ability of the microwave system to detect non-visible plastics within trimmed beef meat samples on a moving conveyor system as depicted in Fig. 29.

Figure 29. Phantom 2 was designed by using trimmed beef samples with non-visible plastic hidden within meat samples (various size and locations were tested) on a conveyor system.

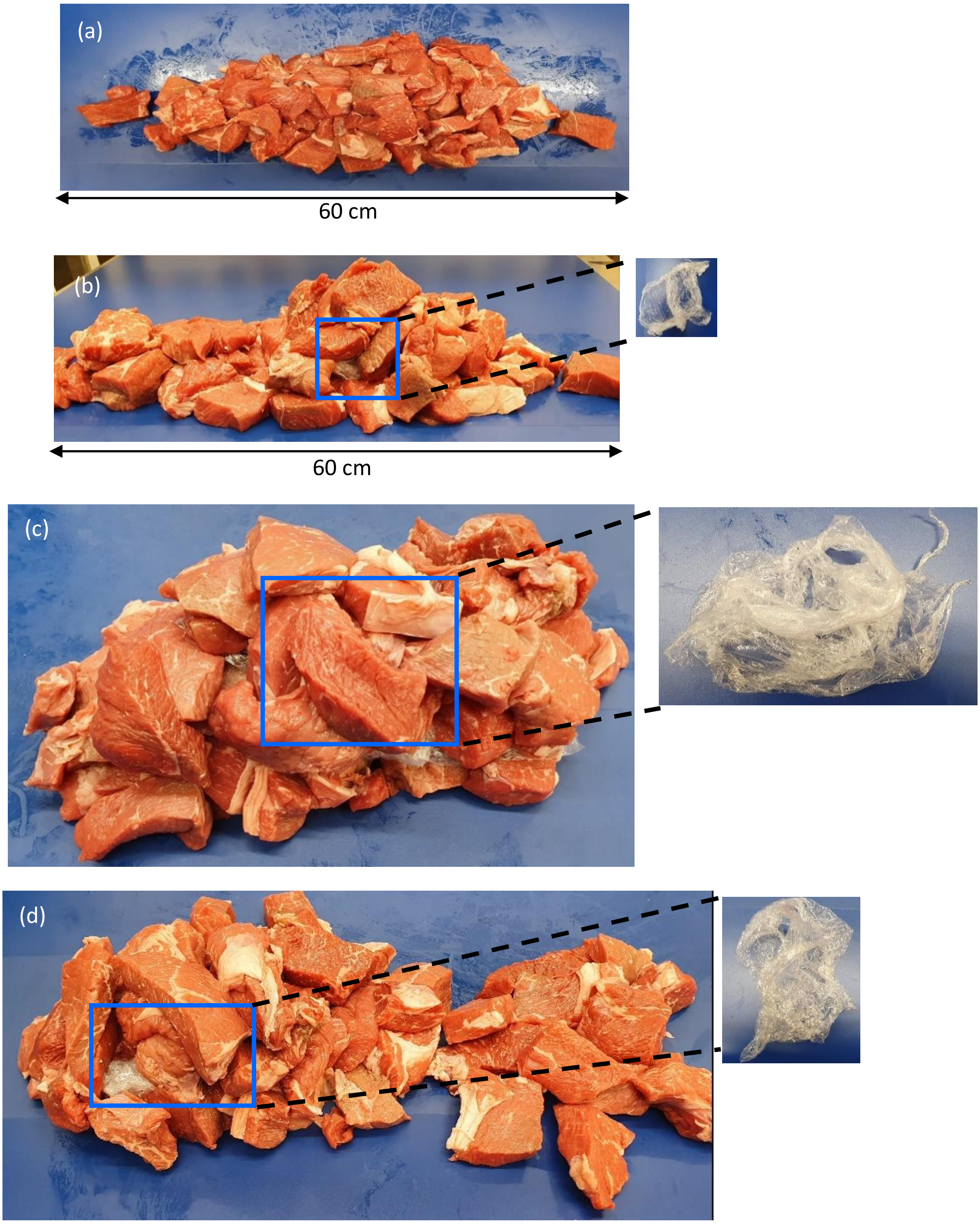

4.6 Data acquisition

A monostatic mode was used to acquire an image of the meat phantoms on the conveyor system, comprising of the 8-antenna of the planar array (Fig. 30). The UWB pulses are generated using the VNA in a step-frequency manner across the band from 1.0GHz to 6.5GHz. The data (complex S-parameters) are collected by activating Port #1 to Port #8 on time interval of one second and the PC to record the data from the 8-antenna element of the planar array, S11, S22, S33, S44, S55, S66, S77 or S88 as shown in Fig. 27(a) and 27(b).

The scanning systems are controlled by Python codes based on the speed of the conveyor systems. In this experiment the conveyor system was set at 4.3cm/s speed with scanning of 13 measurements for 13.75s. For every 4cm, microwave scanning via eight antennas was performed. The monostatic approach was chosen as it has so far given satisfactory results and avoids the complexity in hardware and software required for a multi-static approach. The object (rectangular meat phantom with plastic) was placed on the platform as shown in the Fig. 30.

Figure 30. Microwave array with meat phantom 1 in situ.

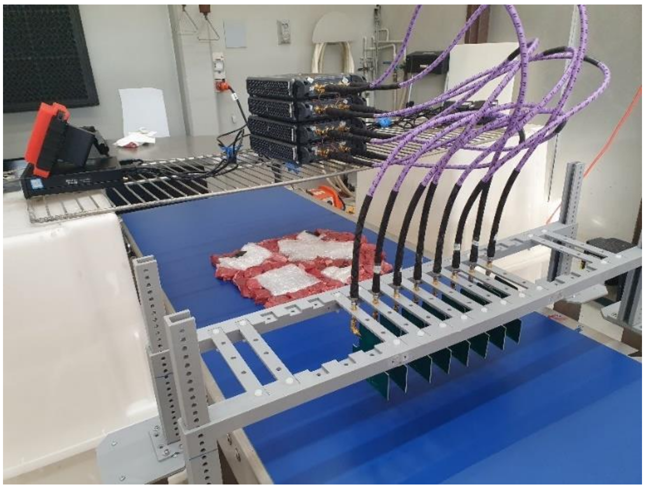

All the 8 antenna elements are used as transmitters and receivers. Initial data for the 4 ports (S11, S22, S33, S44, S55, S66, S77 and S88) of the VNA are recorded when there is no meat phantom present in the platform as shown in Fig. 25. These data are subsequently used to remove reflections caused by the conveyor system.

Initial calibrating measurements are taken without any phantom, to record the performance of the horn and Vivaldi patch antenna in free space while in the array platform on the conveyor system as shown in Fig. 31 (a1 and b1) for horn antenna and Fig. 32 (a1 and b1) for Vivaldi antenna.

The meat phantoms were then scanned using both the horn and Vivaldi array systems. Fig. 31(a2 and b2) and Fig. 32(a2 and b2) shows the measured reflection coefficient of horn and Vivaldi antenna. Fig. 31 (a3 and b3) and Fig. 32 (a3 and b3) show the processed magnitude of frequency domain signals for horn and Vivaldi patch antenna. The time domain analysis is depicted in Fig. 33 for horn and Vivaldi antenna based on processed magnitude of frequency domain signals.

Figure 31. The measured and processed frequency domain reflection coefficient (Left (a): S11, S22, S33, S44) and (Right (b): S55, S66, S77, S88) for eight horn antennas in linear array platform on conveyor system at sixth (6) measurement of Figure 28(a). (a1 & b1) without any phantom (a2 & b2) with phantom as shown in Figure 28(a) measurement 6. (a3 & b3) the processed reflection coefficient.

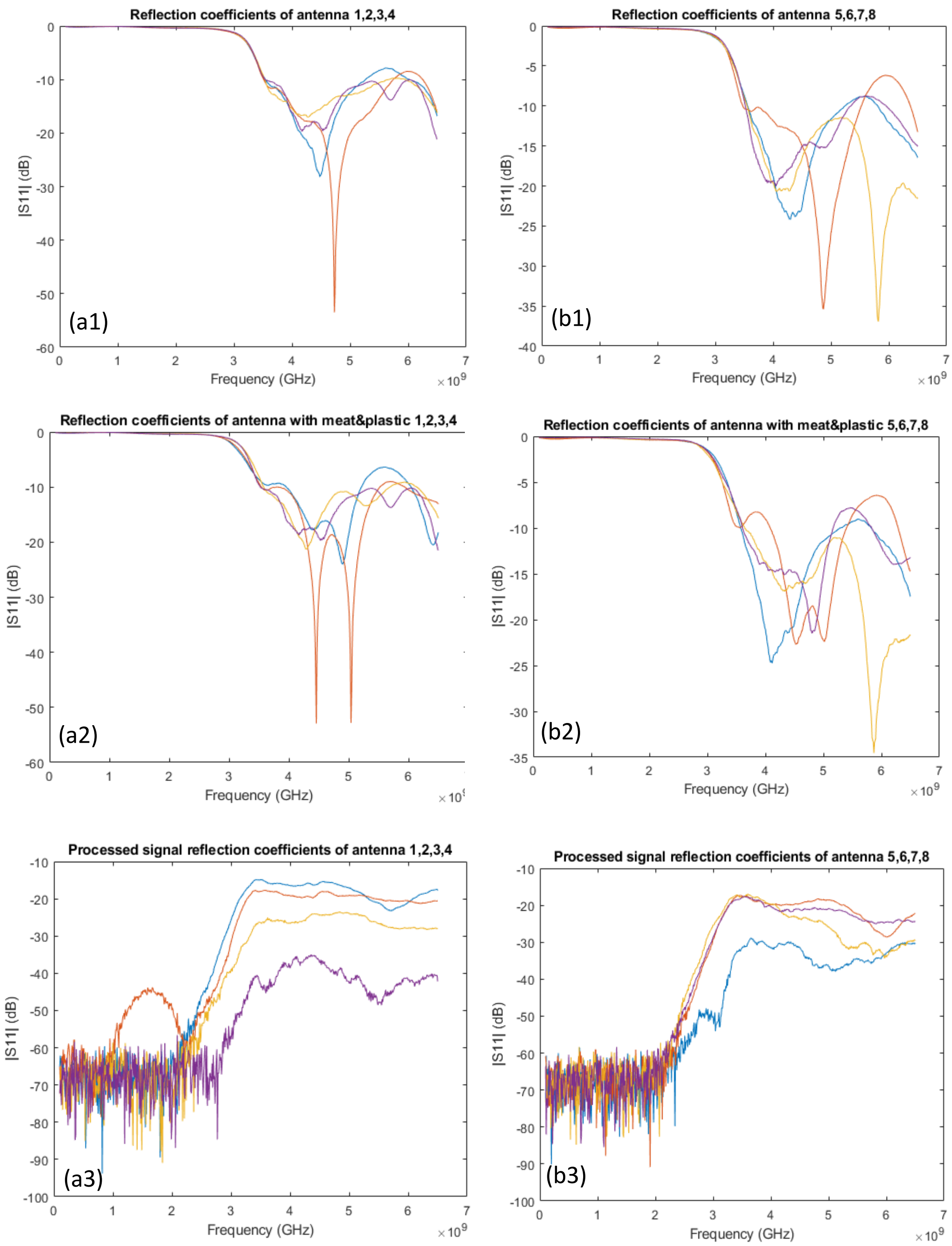

Figure 32. The measured and processed frequency domain reflection coefficient (Left (a): S11, S22, S33, S44) and (Right (b): S55, S66, S77, S88) for eight Vivaldi patch antennas in linear array platform on conveyor system at sixth (6) measurement of Figure 28(b). (a1 & b1) without any phantom (a2 & b2) with phantom as shown in Figure 28(b) measurement 6. (a3 & b3) the processed reflection coefficient.

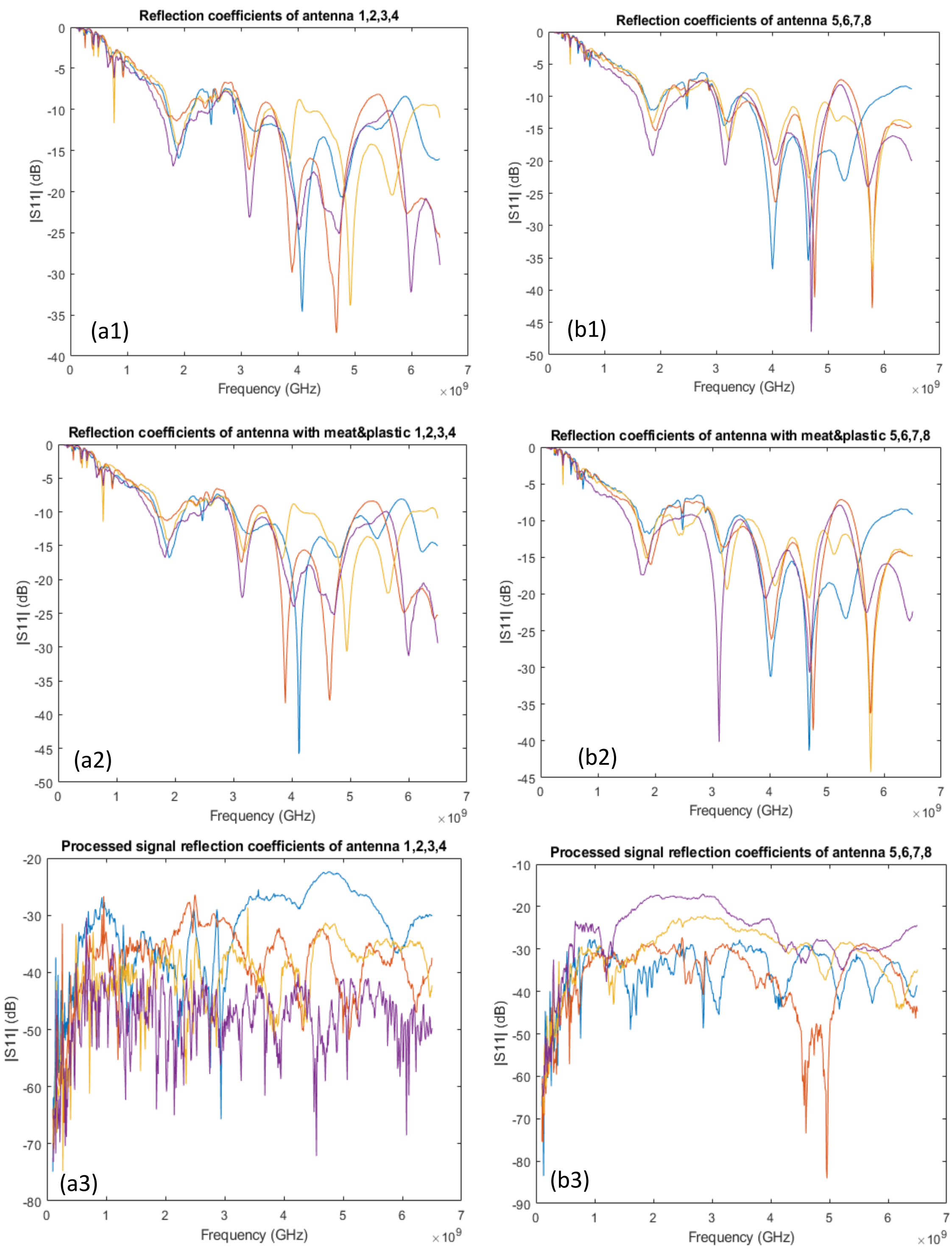

Figure 33. The processed time domain of reflection coefficient (Left (a): S11, S22, S33, S44) and (Right (b): S55, S66, S77, S88) antennas at sixth measurement point on automated conveyor system by using). (a1 & b1) horn antenna array system (a2 & b2) Vivaldi patch antenna array system

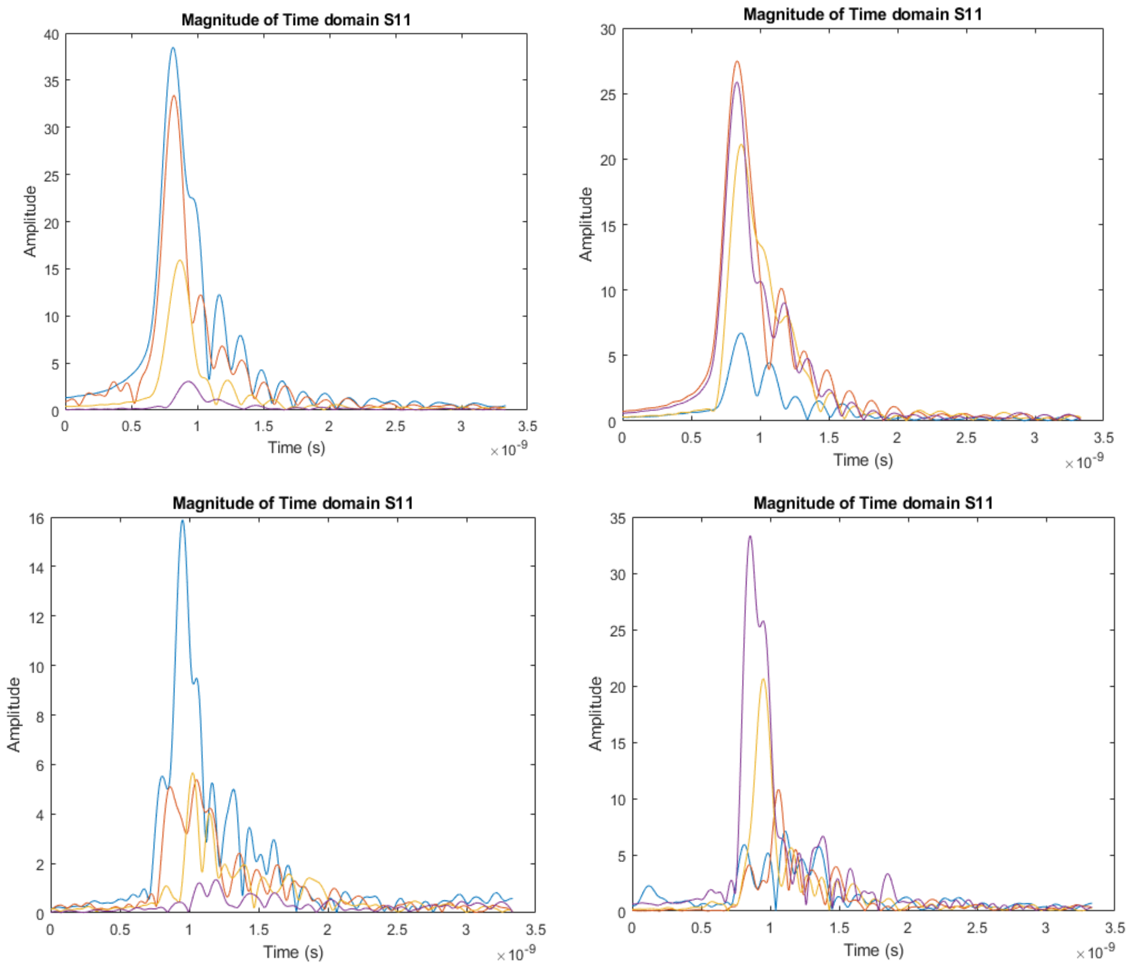

4.7 Microwave Imaging

The eight ports of the VNA (Port #1, Port #2, Port #3, Port #4, Port #5, Port #6, Port #7 and Port #8) were calibrated across the proposed UWB frequency using 3 standards prior to microwave scanning.

4.7.1 Optimisation-based propagation technique

Following the data collection, a post-processing algorithm was applied to reconstruct the images by using modified delay-and-sum confocal algorithm (Ireland & Bialkowski, 2011) as detailed in section 3.3. The confocal imaging algorithm was further improved based on optimisation-based propagation techniques (L. Guo & A. Abbosh, 2015) to locate the hidden plastics within trimmed beef meat chunks in this study. The proposed techniques determine the position-dependent dielectric constants based on certain objective equations (Conceição, Mohr, & O'Halloran, 2016).

Beam-formed energy values within the domain *D* are calculated and collated in sub-grids to form the cost function. The technique is robust in automated conveyor system with distributed trimmed beef chunks scenarios with and without visible and non-visible presence of plastics. The technique is formulated as an optimisation problem

$$\epsilon_R^{opt} = \arg\max_{\epsilon_R} \left\{ \frac{\max(\mathbf{G})}{||\mathbf{G}||_1 - \max(\mathbf{G})} \right\}$$

Ω_k is member of *D* and $\varepsilon_R{}^{opt}$ is the optimal relative permittivity to use. $\mathbf{G}$ can be derived from

$$\mathbf{G} = \left[G_1^{sub}, G_2^{sub}, \ldots, G_K^{sub}\right]$$
$$G_k^{sub} = \frac{\sum_r I(r)}{\sum_r \chi_D(r)}, \quad r \in \Omega_k$$

where $\chi_D(.)$ is the indicator function of *D, k* is the subgrid index which pertain to the cells within Ω_k and Ω_k member of *D.* The given objective function is minimised until convergence or a maximum of 56 iterations.

To further test the ability of the proposed system to image multiple scanning of the running conveyor system, Truncated Singular Value Decomposition (TSVD) developed and tested in these studies based on the technique described by Gilmore *et al.* (2009). The TSVD was developed based on time domain signals which obtained by using multiple frequencies.

4.8 Results

The conveyer system imaged without any meat is depicted in Fig. 34. The entire image is blue.

Figure 34. Image of conveyor belt without meat.

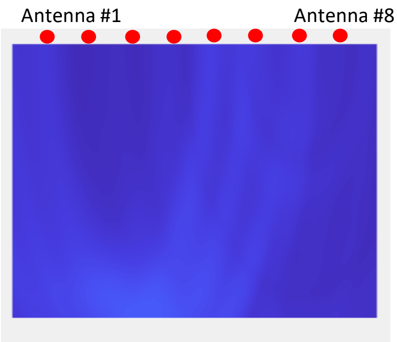

4.8.1 Trimmed beef meat chunks with hidden plastic

The image results from the scanned meat chunks at measurement # 5, #7 and #9 (Fig. 35) are depicted in Fig. 36. These images were obtained while the conveyor was running.

Two techniques were used to derive the images. Technique 1 (Fig 36. a1, b1, c1) was the standard confocal imaging technique. In these images the colours demonstrate that standard confocal imaging has the ability to detect meat, however, the plastic is very difficult to locate as it is masked by the high dielectric profile of the meat. Technique 2 (Fig 36. a2, b2, c2) demonstrates the confocal imaging with an added optimisation-based propagation technique. This technique was able to eliminate the high dielectric profile medium of the meat, focusing exclusively on the plastic which has a low dielectric profile. As demonstrated in the Fig. 36. a2, b2, c2, the amount of yellow noise is reduced enabling clear detection of the plastic foreign body.

Figure 35. Scanning positions using horn antenna on trimmed beef with hidden plastic (as depicted in Fig. 29(b). The dashed straight line represent scanning measurement, #5, #7 & #9. The dashed blue circles show the position of the hidden plastic, position 1 hidden plastic is 2mm thick x 70mm wide, 120mm length. Position 2 hidden plastic is 30 mm thick x 20mm wide x 20mm length.

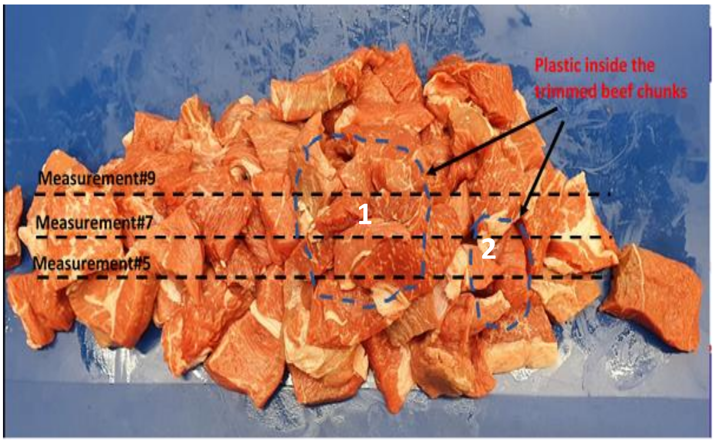

Figure 36. Phantom with hidden plastic (depicted in Fig. 34) at scanning positions (a) measurement #5 (b) measurement #7 (c) measurement #9. Two imaging techniques were used, (1) represents standard confocal imaging technique and (2) represents the confocal imaging with optimisation propagation.

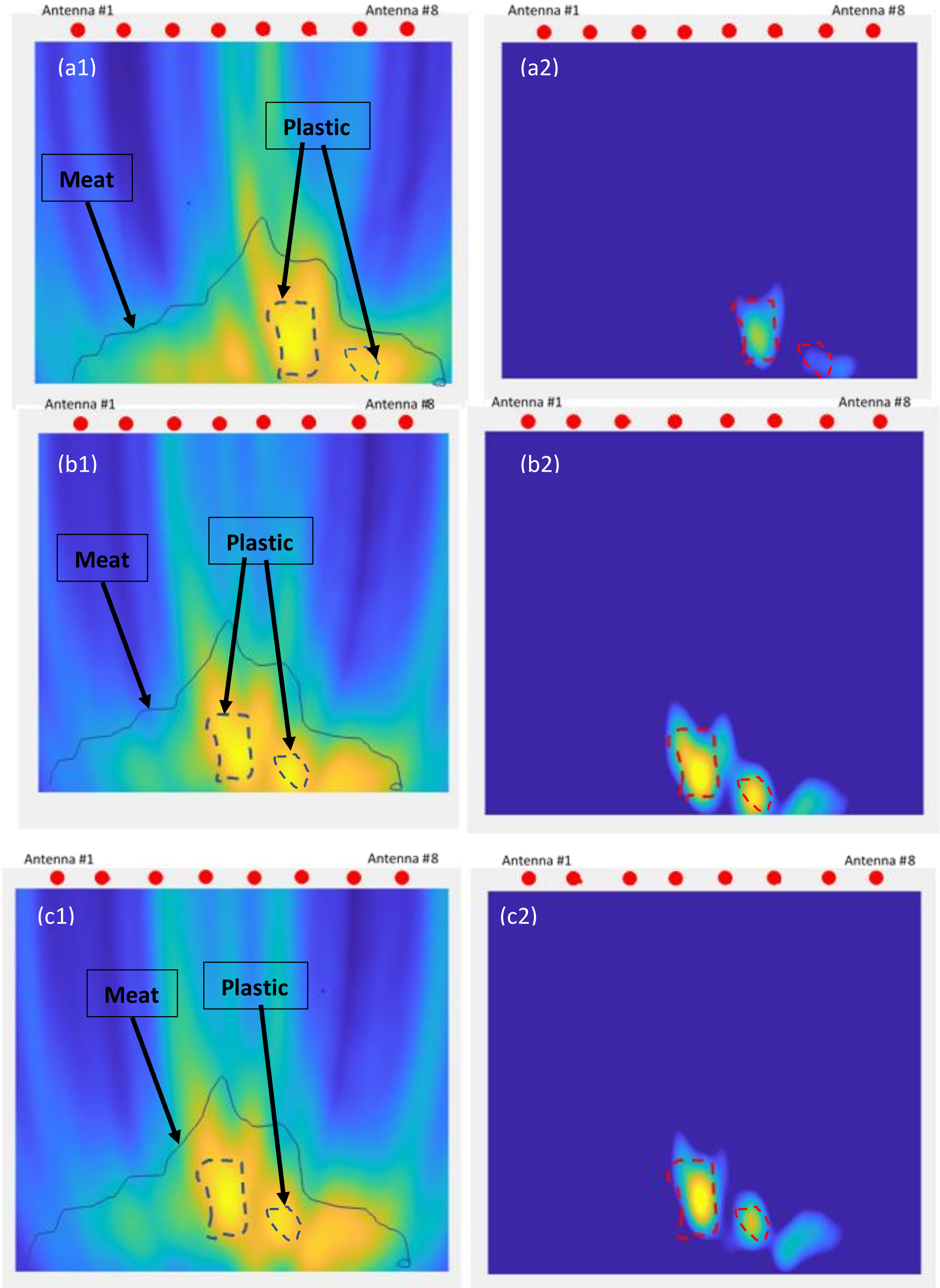

Additional scanning was performed with meat in different configurations aligned along different antennas (Fig. 37), with the images depicted in Fig. 38. Again, the confocal imaging technique was able to detect the contaminants (Fig. 38 a1, b1), however, when the optimised propagation was applied the plastic was able to be clearly differentiated (Fig. 38 a2, b2). The precision of detection was similar to the results in Fig. 36.

Figure 37. Configurations of meat chunks with hidden plastic. The dashed circles represent the position of the hidden meat in (a) the plastic was 40 mm thick x 120 mm wide x 120 mm length and (b) contained hidden plastic 1 = 20 mm thick x 60 mm wide x 60 mm length and hidden plastic 2 = 30 mm thick x 20 mm wide x 20 mm length.

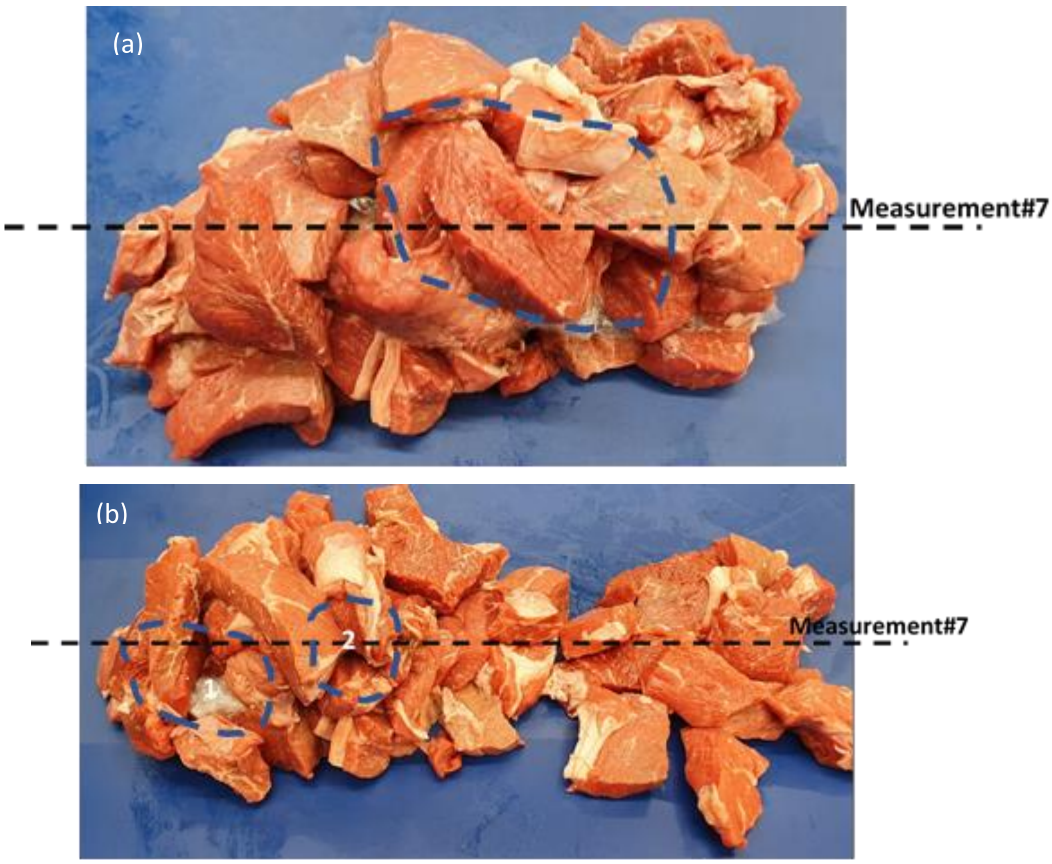

Figure 38. Phantom with hidden plastic at scanning positions (a) 1x hidden plastic (Fig 36.a) and (b) 2x hidden plastic (Fig. 36.b). Two imaging techniques were used, (1) represents standard confocal imaging technique and (2) represents the confocal imaging with optimisation propagation.

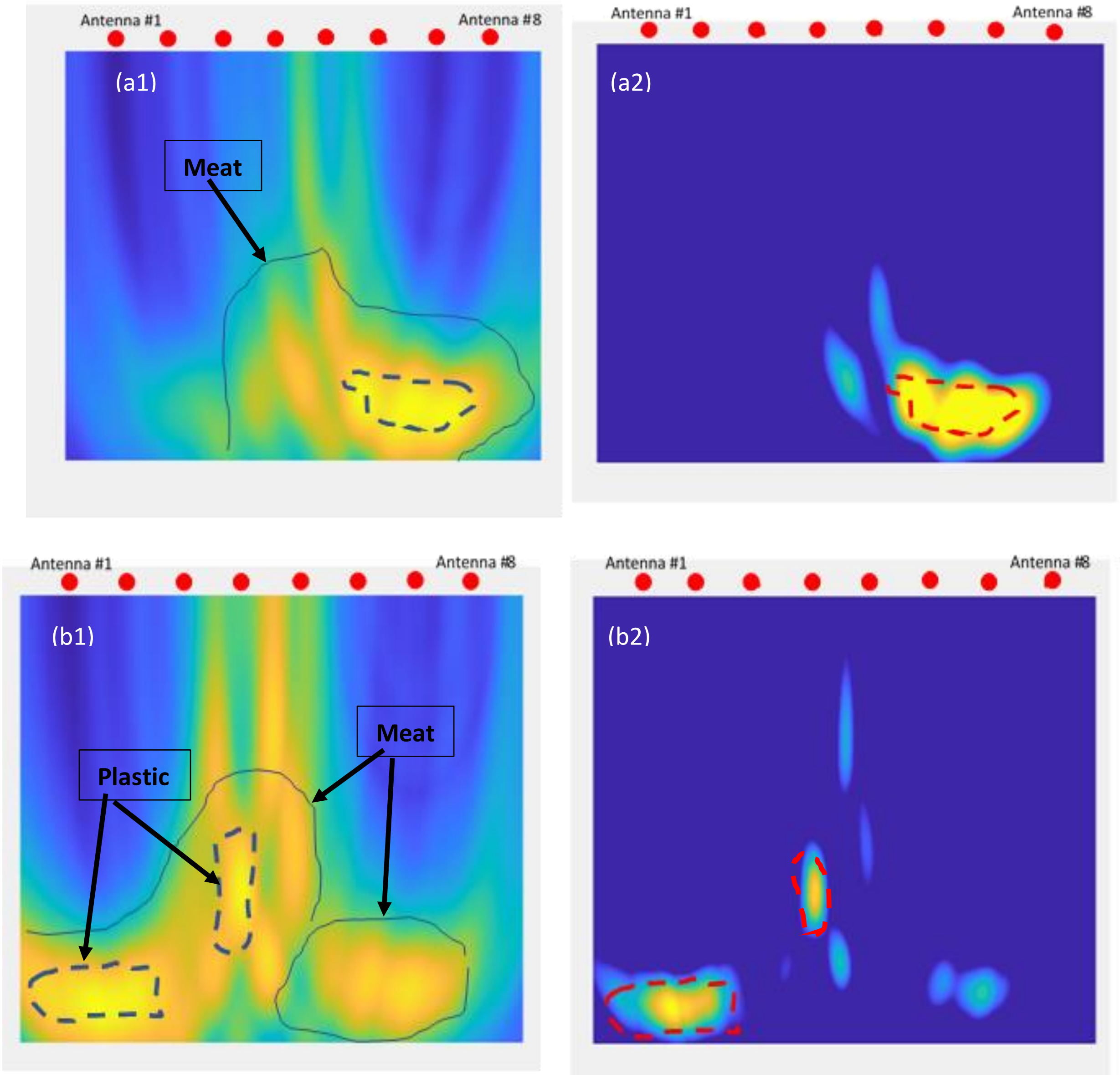

4.8.2 Trimmed beef meat chunks with visible plastic

The results using the new TVSD algorithm technique are depicted in Fig. 39. These images were derived at all 13 measurement positions, when the conveyor was running.

The yellow colour represent plastic, based on its low dielectric properties. For every measurement position, the visible foreign body plastic was able to be correctly detected.

Figure 39. Images of various scanning position of phantom in 28(a). (a) The phantom with plastics and measurements position by using array of horn antenna as the conveyor system run at speed 4.3cm/s. The images show the measurements points of the phantom.

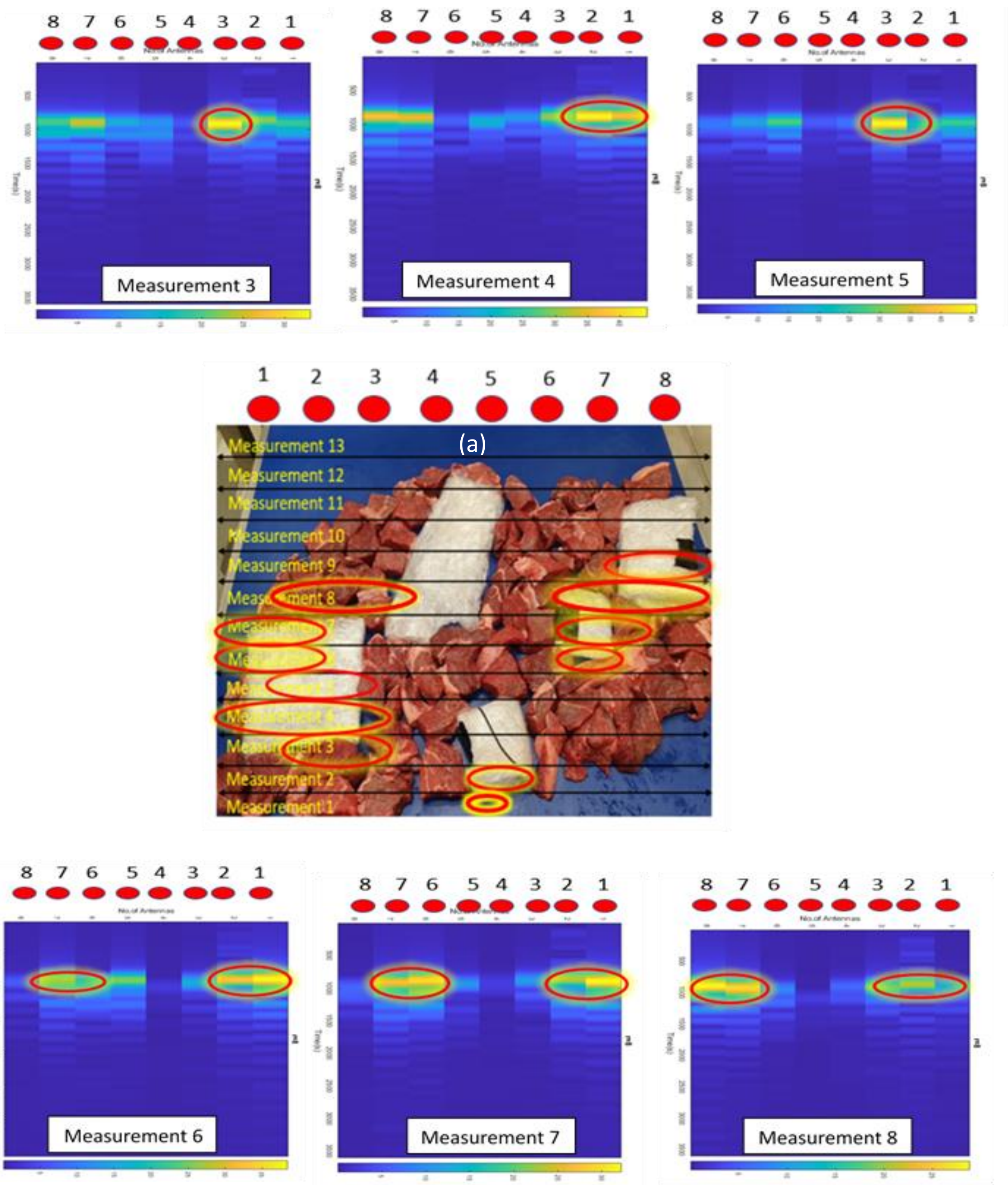

6 Discussion and Conclusion

Plastic foreign bodies, within beef (boxed and on or under loose chunks) were successfully identified by the microwave array imaging system.

Experiment 1 assessed microwave detection of plastic within boxed meat. Three different phantoms of varying lean meat to fat ratios were constructed, 100% lean, 80% lean + 20% fat, and 60% lean + 40% fat. Within these phantoms three different configurations of embedding plastic were tested to assess different plastic sizes and locations within the boxed meat. Microwave scanning using a confocal imaging technique successfully detected plastic embedded within boxed meat trim containing between 60 – 95% chemical lean.

Experiment 2 assessed microwave detection of plastic in unboxed meat on a food grade automated conveyor system. Within chunks of meat distributed along a conveyor belt, two configurations of plastic foreign bodies were assessed being visible or non-visible. The meat was scanned by an array of 8 antennas as it moved along a conveyor belt.

Microwave array using a confocal imaging technique with optimisation-based propagation successfully detected non-visible plastic embedded within loose beef meat chunks on a conveyor belt running at commercial speeds.

Microwave array using Truncated Singular Value Decomposition (TSVD) successfully detected visible plastic embedded within loose beef meat chunks on a conveyor belt running at commercial speeds.

The improved confocal algorithm technique using optimisation-based propagation was able to remove the dielectric noise from meat and air, to focus at locating only the plastic. This optimised the image, enabling clear differentiation of plastic contaminants from meat.

The new TVSD algorithm demonstrated success as an online imaging technique for all 13 measurements taken in real time.

7 Recommendations

This project has demonstrated that microwave imaging can detect plastic within boxed trim of varying lean-fat ratios, and that it can detect plastic when visible or under loose beef trim on a conveyor moving at commercial speeds. Future commercial testing of a microwave array for foreign body plastic detection would include;

- Fine tuning of the algorithm to eliminate air-gap image noise when scanning loose beef trim
- Testing smaller configurations of plastic embedded within meat phantoms and loose beef trim at the speed of an industrial conveyor
- Undertaking a larger “error-rate” study in a commercial environment where meat trim is deliberately seeded at intervals with contaminants to determine frequency of positive and false-positive detection.

8 References

Aladjadjiyan, A. (2006). Physical hazards in the agri-food chain. *Safety in the agri-food chain*, 209-222.

Bourqui, J., Okoniewski, M., & Fear, E. C. (2007). Balanced antipodal Vivaldi antenna for breast cancer detection. doi: 10.1049/ic.2007.1262

Cavalheiro, C. P., da Silva, M. C. A., Leite, J. S. F., da Silva Felix, S. K. R., Herrero, A. M., & Ruiz-Capillas, C. (2020). Physical hazards in meat products: Consumers' complaints found on a Brazilian website. *Food Control, 108*, 106892. doi: 10.1016/j.foodcont.2019.106892

Chen, Q., Zhang, C., Zhao, J., & Ouyang, Q. (2013). Recent advances in emerging imaging techniques for non-destructive detection of food quality and safety. *TrAC Trends in Analytical Chemistry, 52*, 261-274. doi: 10.1016/j.trac.2013.09.007

Conceição, R. C., Mohr, J. J., & O'Halloran, M. (2016). *An introduction to microwave imaging for breast cancer detection*: Springer.

Datta, A. K. (2001). *Handbook of microwave technology for food application*: CRC Press.

Edwards, M. (2004). *Detecting foreign bodies in food*: Elsevier.

Gilmore, C., Mojabi, P., Zakaria, A., Ostadrahimi, M., Kaye, C., Noghanian, S., Shafai, L., Pistorius, S., & LoVetri, J. (2009). A wideband microwave tomography system with a novel frequency selection procedure. *IEEE Transactions on Biomedical Engineering, 57*(4), 894-904.

Ireland, D., & Bialkowski, M. E. (2011). Microwave head imaging for stroke detection. *Progress In Electromagnetics Research, 21*, 163-175.

Langley, J., Hall, P., & Newham, P. (1996). Balanced antipodal Vivaldi antenna for wide bandwidth phased arrays. *IEE Proceedings-Microwaves, Antennas and Propagation, 143*(2), 97-102. doi: 10.1049/ip-map:19960260

Marimuthu, J. (2016). *Design of wideband microwave frontend for microwave-based imaging systems.* PhD thesis, The University of Queensland, Brisbane.

Pozar, D. M. (2005). Microwave Engineering, Chapter 8. *John Wiley & Sons, Hoboken, New Jersey, 3*, 91-93.